



**Fys - 3921**  
**Master's Thesis in Electrical**  
**Engineering**

---

Fluid-Thermal properties of electromagnetic  
heated water boli used in thermal treatment of  
superficial cancer

Enrique Luis de la Cruz Martínez

June, 2007

Faculty of Science  
Department of Physics and Technology  
University of Tromsø



Fys - 3921  
Master's Thesis in Electrical Engineering

Fluid-Thermal properties of electromagnetic  
heated water boli used in thermal treatment of  
superficial cancer

Enrique Luis de la Cruz Martínez

June,2007



I like to think in this project as a clinical medium to reach what a person, I  
would have liked to meet, used to say:

*“A quitar cosas feas”*

Enrique de la Cruz Matton



# Acknowledgements

I would like to thank first of all to Svein Jacobsen, who has been very patient and has showed me how hard it is to be a scientist. I have learned a lot with him and the most important, though some really stressing days, I have enjoyed this work.

I'm sorry for the non Spanish speaking but I would like to write the rest of the acknowledgements in my mother tongue to be able to make this master thesis a bit more personal.

Me gustaría dar las gracias a mi familia y más concretamente a mis padres, que han hecho posible que llegue este momento. Gracias por tener paciencia y comprender que en Teleco no se aprueba todo a la primera, ni a la segunda, ni. . . Sobre todo quiero daros las gracias por haber hecho este último esfuerzo de traerme ni más ni menos que a Noruega a estudiar durante todo un año, ofreciéndome la oportunidad de conocer a muchísima gente nueva y darme recuerdos que nunca olvidaré.

Por supuesto a mis tetes, también quiero agradecerles todos los días que hemos hablado durante mi estancia aquí en Tromsø, haciéndome sentir de nuevo como en casa en días en los que los echaba de menos (Pablo, cuando leas esto te dejo darme un solo abrazo).

Finalmente, te quiero dar las gracias a ti, María. Muchas gracias por haberme animado esos días en los que volvía a casa destrozado porque nada del proyecto funcionaba, pero sobre todo por haberme dado el año más precioso de mi vida a tu lado.



# Contents

<b>1</b>	<b>Introduction</b>	<b>1</b>
<b>2</b>	<b>Methodology</b>	<b>9</b>
2.1	Theoretical approach of the water flow . . . . .	9
2.1.1	Navier-Stokes equations . . . . .	9
2.1.2	Darcy's law . . . . .	10
2.1.3	Brinkman equations . . . . .	11
2.1.4	Turbulence in the flow . . . . .	12
2.2	Theoretical approach of the temperature distribution . . . . .	14
2.2.1	Conduction . . . . .	15
2.2.2	Convection . . . . .	15
2.2.3	Penne's bioheat equation . . . . .	16
2.3	Applicator model . . . . .	16
2.4	Antenna applicator . . . . .	20
2.4.1	Antenna configuration . . . . .	20
2.5	Computational tools . . . . .	21
<b>3</b>	<b>Results</b>	<b>29</b>
3.1	Tube water flow . . . . .	29
3.1.1	Raynold's number for the tube . . . . .	29
3.1.2	Flow behavior in the model . . . . .	30
3.2	Velocity field in the bolus . . . . .	31
3.3	Temperature distribution . . . . .	34
3.3.1	Temperature of the model in a controlled environment	34
3.3.2	Temperature distribution of the transeiving heating antenna . . . . .	35
3.3.3	Fluid velocity influence on temperature distribution of the final model . . . . .	43
<b>4</b>	<b>Discussions</b>	<b>51</b>
4.1	Tube water flow . . . . .	51

4.2	Velocity field in the bolus . . . . .	52
4.3	Temperature distribution . . . . .	52
4.3.1	Temperature of the model in a controlled environment	52
4.3.2	Temperature distribution of the transceiving heating antenna . . . . .	53
4.3.3	Fluid velocity influence on temperature distribution of the final model . . . . .	54
<b>5</b>	<b>Conclusions</b>	<b>57</b>
5.1	Final conclusions about the results . . . . .	57
5.2	Further simulations and improvements in the model . . . . .	58

# List of Figures

1.1	Scheme of a system for local hyperthermia. Applicator position and power output can be varied until a clinically satisfactory adjustment is achieved [10] . . . . .	3
1.2	Regional hyperthermia applicator [10] . . . . .	4
1.3	whole-body hyperthermia applicator [10] . . . . .	6
2.1	General flow diagram applied in Darcy’s law. . . . .	11
2.2	Velocity profile inside a circular pipe with laminar flow. . . . .	12
2.3	Velocity profile inside a circular pipe with turbulent flow. . . . .	13
2.4	General representation of non-invasive hyperthermia model. . . . .	18
2.5	3D model with the corresponding equations for each sub-domain. . . . .	19
2.6	Sketch of the dual-mode transceiving antenna [7]. . . . .	20
2.7	Central vertical cut of the configuration including the applicator and tissue [7]. . . . .	21
2.8	List of modules in COMSOL Multiphysics®. . . . .	22
2.9	Photo of the real model . . . . .	23
2.10	Erroneous flow simulation. . . . .	24
2.11	Tube architecture of previous model. . . . .	24
2.12	T piece of the tubes. . . . .	25
2.13	Final model. . . . .	25
2.14	Meshing of first piece of the tube. . . . .	26
2.15	Meshing of the “T” tube. . . . .	26
2.16	Meshing of bolus and PVC layer . . . . .	27
2.17	Total Meshing of the model. . . . .	27
3.1	Flow rate along the input and output tubes. . . . .	30
3.2	Flow cross-section and output in the first hole. . . . .	31
3.3	Positioning of the different lateral plot sections. . . . .	32
3.4	Flow rate in the y and x directions in the center of the bolus. . . . .	33
3.5	Laminar flow in the center of the bolus. . . . .	33
3.6	Bolus temperature distribution in the x and y direction when loaded by air. . . . .	35

3.7	Bolus temperature distribution in the x and y direction when air and tissue loaded. . . . .	36
3.8	Temperature distribution for one transceiving antenna. . . . .	36
3.9	Bolus temperature distribution in the x and y direction. . . . .	37
3.10	Transversal temperature section under the antenna. . . . .	37
3.11	Temperature distribution at different depths under two of the lobes of the antenna. . . . .	38
3.12	Temperature distribution for one heating antenna in the bolus with and without skin. . . . .	39
3.13	Bolus temperature distribution in the x and y direction for different antenna separation. . . . .	40
3.14	Skin temperature distribution in the x and y direction for different antenna separation. . . . .	40
3.15	Tissue temperature distribution in the x and y direction at 6.95 mm depth for different antenna separation. . . . .	41
3.16	Tissue temperature distribution in the x and y direction at 10 mm depth for different antenna separation. . . . .	41
3.17	Temperature distribution at different depths depending on antenna separation. . . . .	42
3.18	Temp in the bolus depending on the velocity. . . . .	43
3.19	Temp in the skin depending on velocity. . . . .	44
3.20	Temp in the tissue at 6.95 mm depth depending on velocity. . . . .	45
3.21	Temp in the tissue at 10 mm depth depending on the velocity. . . . .	45
3.22	Positioning of the different transversal plot sections. . . . .	46
3.23	Transversal temperature distribution under each antenna depending on flow velocity. . . . .	47
3.24	Temperature distributions in depth vs. lateral position. . . . .	48
3.25	Antenna array as distributed in the model. . . . .	49
5.1	L shaped bolus with its different layers . . . . .	59

# Chapter 1

## Introduction

Talking about diseases, it is very rare not to hear the word “cancer” in daily conversation. The reason is that there are more than 10 million cases every year and it has become one of the most devastating diseases in the world, especially in developed countries [1]. A sign of this is that almost everyone can refer to a relative that has been affected. In Norway, one in three gets cancer during his/her lifetime.

The cancer causes and types vary in different geographical regions, but there is always one common characteristic for all these illnesses: alterations in the DNA of cells which has as a consequence an uncontrolled division and growth of them. Almost all these alterations imply changes in the nucleic acid that has a very dangerous impact on the human body [2]. This undesired behavior is characterized by uncontrolled division of cells and the ability of these cells to invade other tissues. This invasion can happen either by direct growth into adjacent tissue through invasion or in a distant place through metastasis.

Metastasis is the stage in which cancer cells are transported through the bloodstream or lymphatic system and thus spread to other parts of the body than the primary focus. Cancer may affect people at all ages, but the risk increases with age, because the DNA damage is more apparent in aging DNA [3].

With development in new technology, we have reached the question: why haven't we found a cure for cancer yet?

The main problem is that there are many kinds of cancers, so it is very difficult to find a general cure, since the treatments vary with type of cancer and location. The most known therapies for treating cancer diseases nowadays are radiotherapy and chemotherapy. However these treatments have many negative side effects, so it is very important to find alternatives which allow the patient to fight the illness without any other consequences or symptoms

than the ones from the cancer itself. For example, radiation therapy side effects are hair loss, fatigue / malaise, low blood count, skin desquamation or mucosity development. For chemotherapy the most common side effects are nausea and vomiting, hair loss, and bone-marrow depression [4].

A possible complementary treatment that is under development is denoted hyperthermia. The basic idea behind this treatment is to create an artificial “fever” of 41 – 45°C in the body of the patient without damaging the benign tissue. Hyperthermia is the cancer treatment this master thesis is focused on. It is also denoted thermal therapy [6] or thermotherapy [5], and is a type of cancer treatment in which it is tried to reach cytotoxic temperatures ( $> 42^{\circ}\text{C}$ ) during approximately 60 minutes [7]. Different studies have shown that moderate temperatures can damage and kill cancer cells, usually with minimal injury to normal tissues. By killing cancer cells and damaging proteins and structures within cells, hyperthermia may contract tumours.

Nevertheless, hyperthermia is still under study in clinical trials and is not widely available yet at clinical institutions [8]. It is almost always used as a complement to other types of cancer therapy, such as radiation therapy and chemotherapy. Hyperthermia makes some cancer cells more sensitive to radiation or even damage other cancer cells that are insensitive to radiation.

When these two techniques are combined, they are often given within an hour of each other when radiotherapy is used or when the choice is chemotherapy. Hyperthermia can also enhance the effects of certain anticancer drugs. The combination of hyperthermia with these therapies has been conducted for many kinds of cancers, including sarcoma, melanoma, and cancers of the head and neck, brain, lung, esophagus, breast, bladder, rectum, liver, appendix, cervix, and peritoneal lining (mesothelioma) [9].

The reason why hyperthermia is not considered as a stand-alone treatment against cancer by the medical community is because not all of the studies made, although many, showed a significant reduction in tumour size or an increased survival in patients receiving the combined treatment [5]. However, there are others reporting high success in this coupling like the study made by Van der Zee *et al.* 1999, where a complete response increase of hyperthermia was observed for breast cancer from 31% to 65% or by Vernon *et al.* 1996 and Jones *et al.* 2005, who observed similar improvements in multi-institutional random [7].

Several methods of hyperthermia are currently under study, including local, regional, and whole-body hyperthermia [9]. In local hyperthermia, heat is applied to a small area, delivering energy to heat the tumour. There are many ways to apply this energy such as microwave, radiofrequency, and ultrasound. Depending on the tumour location, there are several kinds of local hyperthermia methods: external, regional and whole-body hyperthermia [10].

External hyperthermia is used to treat tumours that are in or just below the skin (superficial), where non-invasive applicators are located around or near the appropriate region, and energy is focused in the tumour to increase its temperature, as shown in Figure 1.1. Also talking about external hyperthermia, there are two techniques that should be distinguished depending on the location of the tumour. The first is the intraluminal or endocavitary method used for treatment in or near body cavities, like the esophagus or rectum, in which probes are placed inside the cavity and inserted into the tumour to heat the volume directly [10].

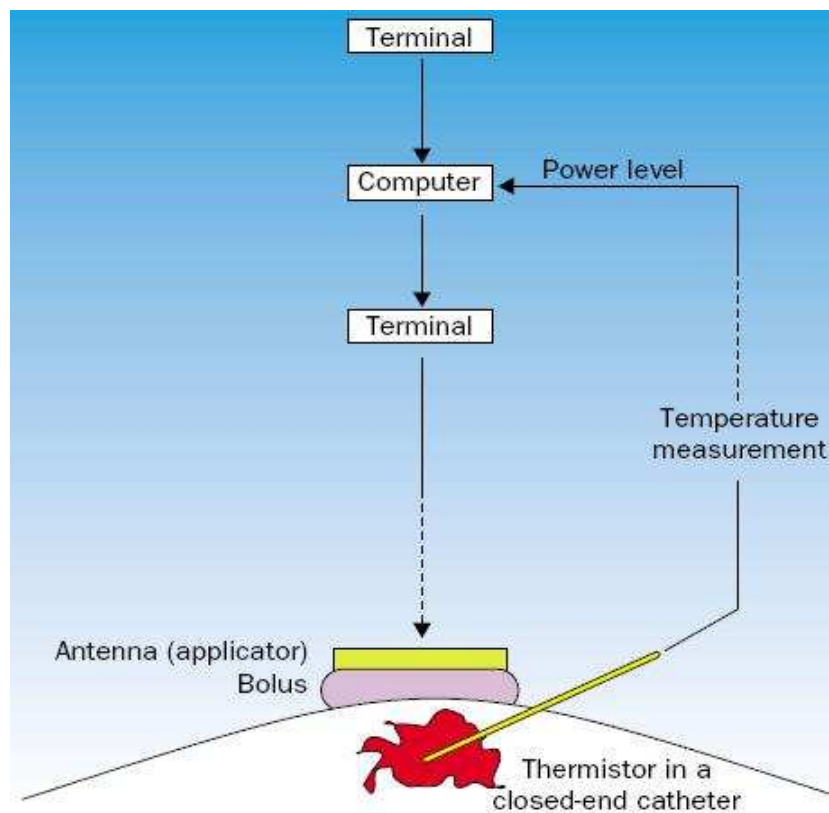


Figure 1.1: Scheme of a system for local hyperthermia. Applicator position and power output can be varied until a clinically satisfactory adjustment is achieved [10]

If the tumour is located deep within the body, like brain tumours, the technique used is denoted interstitial (invasive). It allows heating of the tumour more effectively than non-invasive techniques do. In this method, probes or needles are inserted into the tumour, always under anaesthesia.

Since the locations could be in very delicate places, as the brain is, it is very important to be very accurate during operation. This is why imaging techniques as ultrasounds are used to aim the probe in a proper position within the tumour [10]. One of these techniques is radiofrequency ablation (RFA) where radio waves are used to heat and kill the cancer cells, by inducing temperatures up to  $50 - 120^{\circ}\text{C}$  [11].

Another kind of local hyperthermia is regional hyperthermia, where we can again make some distinctions depending on the position of the tumour and the technique used. These methods include the “deep-tissue” approach, the regional perfusion and the continuous hyperthermic peritoneal perfusion (CHPP) techniques. In general they are all applied to heat large volumes of tissue, such as a body cavity, organ, or limb [12].

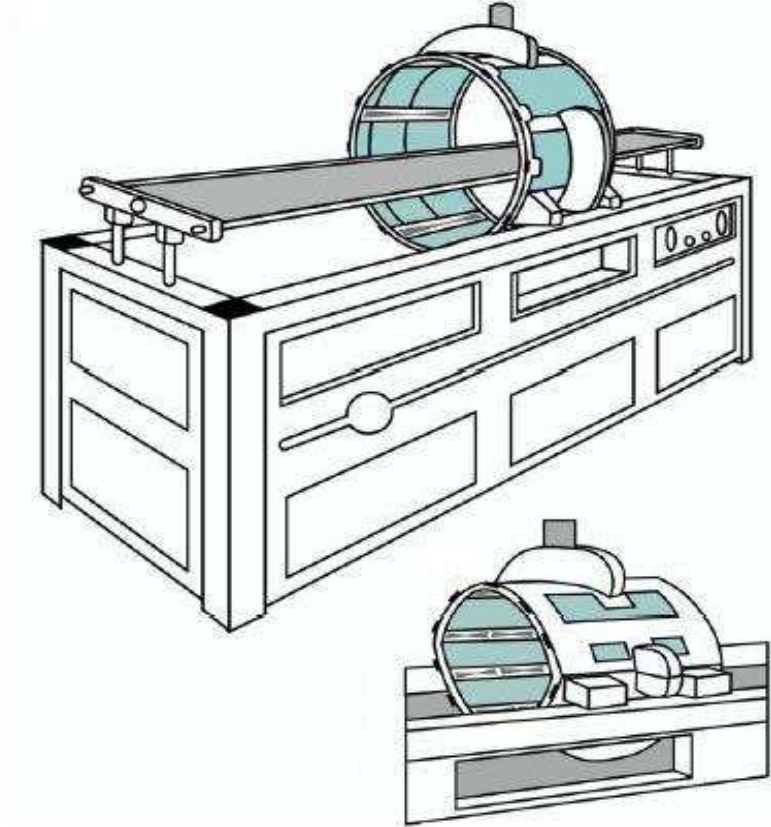


Figure 1.2: Regional hyperthermia applicator [10]

The CHPP is a technique used to treat cancers within the peritoneal cavity (the space within the abdomen that contains the intestines, stomach, and liver), including primary peritoneal mesothelioma and stomach cancer.

During surgery, heated anticancer drugs flow from a heating device through the peritoneal cavity. The peritoneal cavity temperature reaches 41 – 42°C [12].

Deep tissue approaches may be used to treat cancers within the body, such as cervical or bladder cancer. External applicators are positioned around the body cavity or organ to be treated, and microwave or radiofrequency energy is focused on the area to raise the cell temperature [10].

Regional perfusion techniques can be used to treat cancers in the arms and legs, such as melanoma, or cancer in some organs, such as the liver or lung. Here some of the patients blood is extracted, heated, and then pumped (perfused) back into the limb or organ. All this is normally done together with an anticancer drug treatment [13].

The last of the hyperthermia treatments is whole-body hyperthermia, which is used to treat metastases, since there is no concrete location of the cancer and the treatment used has to be in the whole body. This can be accomplished by several techniques that raise the body temperature to about 41.8°C using thermal chambers or hot water blankets [3].

The type of treatment we are focusing on in this study is less aggressive than any of the ones mentioned above. The basis of this treatment is to heat the area where the tumour is located, producing greatest effects to areas with poor blood circulation, because the blood is capable to reduce this accumulate heat in the benign tissue. Several studies have estimated the effects of heat removal by the blood flow and of heat loss from the tissue surface by thermal convection. Thus the goal of local hyperthermia is to reach the highest non-traumatic temperature possible as a threshold, over which benign tissue begins to be damaged, in order to debilitate the tumour and ensure the effectiveness of the other treatments.

High temperature in the body is often reached using microwave radiation by trying to emulate the precise environmental conditions in order to reach the most efficient results against the cancer and without damaging the normal tissue. To achieve our goal, the key quantity needed to be known is the induced electromagnetic field (power deposition pattern) inside the irradiated biomass. This pattern will be greatly determined by the permittivity and conductivity of the volume under treatment. With a priori information it would be easier to solve one of the more difficult problems in clinical hyperthermia, which is the determination of the complete temperature distribution throughout both tumour and normal tissues [7].

In this case our attention is focused on non-invasive hyperthermia systems, which are less traumatic to patients and minimizes the risk of mixing abnormal cells with healthy tissues. For that application, the three main applicators used are the reflector-backed dipole, the direct contact applicators

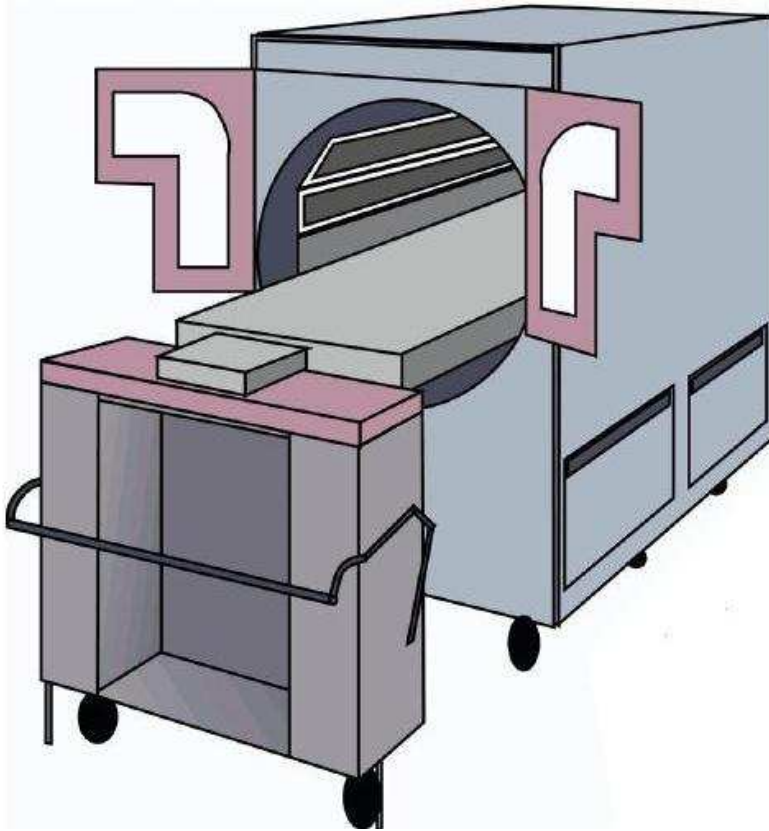


Figure 1.3: whole-body hyperthermia applicator [10]

and the printed circuit antennas. The first one, operating at a frequency of 2450 MHz, is used within a shielded enclosure to increase its effectiveness in heating, but do not produce localized heating [14].

Direct contact applicators, which are generally sections of waveguides or microwave cavities, are placed in contact with the target to be heated and a coupling bolus is usually employed between the applicator and the target, which provides a path for circulation of a cooling fluid. Their primary disadvantage is their large size and weight [14].

Another applicator is the printed circuit board antennas which include microstrip patches, apertures or slots. They have proved to be useful in realization of hyperthermia and offer the advantage of being potentially cheap and flexible enough to adapt themselves to various configurations and with electromagnetic characteristics comparable to other microwave radiators. However, most microstrip circuit designs are restricted to medium power levels only ( $< 60 - 70W$ ). Also, the near-zone electric fields of these antennas

are predominantly normal to the applicator face, and may cause undesired preferential heating at interfaces between layers of the human body [14].

The prototype antenna this master thesis deals with is designed for breast cancer treatment, and thus printed antennas are used in order to make the design lightweight and adaptable to contoured surfaces [14]. The system uses multiple antennas in order to obtain an homogeneous temperature distribution in the treated tissue. The goal of this project is to analyze the effect that the heat deposition of this array has in the coupling bolus between the antennas and the patient. The bolus is cooled by the flow of deionized (DI) water at about 42°C and at a certain water mass flow rate. The bolus thickness and water temperature is fixed for having an optimum performance [7], but a study of how the flow influences in the heat distribution has not been studied.

In previous studies (Jacobsen S *et al.* 2007), a smaller model (4cm x 6cm) of the bolus behavior was used due to heavy computational limitations. Thanks to availability of new computer resources, a more realistic simulation can be made of the temperature distribution in the volume of the bolus and thus to obtain more reliable information on the influence that the bolus has on the temperature distribution within the tissue. This is very important since a continuous monitoring of the temperature in the tissue is made by the transceiving antennas in order to obtain a feedback and modify appropriately the power. It is crucial to differentiate between the heat caused by the antennas themselves and the heat induced by the water flow of the bolus. Numerical computations can also provide additional information for dose planning, of course with some limitations, since the simulations are made with generic tissue data and not with the specific information of the treated patient [7].

The clinical goal to be reached for any kind of tissue and antenna distribution, concerning the bolus, is to reach homogenous temperature by varying the water flow between feasible limits until the most appropriate solution is found.

To make these simulations I have used COMSOL Multiphysics which is the appropriate tool to apply the Incompressible Navier-Stokes equations, needed to describe the flow of water without obstacles, Brinkman equations, to analyse the flow in inhomogeneous porous media, and the heat equation which will calculate the temperature distribution in the system with the help of the velocity vector obtained from the fluid dynamic equations mentioned before [15]. Hence with these equations, applied to a realistic model of our system, we could set the basis to find the appropriate working conditions for a further development of this technique.



# Chapter 2

## Methodology

### 2.1 Theoretical approach of the water flow

The goal of this project is to make a study of the thermal properties within the bolus and the tissue, by looking at changes in the behavior of the whole volume due to the cooling effect of the water flowing through the bolus. This is one of the largest constraints of this problem, since the dynamic character of the problem requires a lot of computational power. Therefore, the flow part has to be solved initially and then subsequently the thermal problem. The water flow is described by Navier-Stokes equations for water flowing in free space and Darcy's law and Brinkman equations for water flowing in porous media.

A general behavior of the fluid is described by Reynold's number to estimate whether the flow is turbulent or not.

#### 2.1.1 Navier-Stokes equations

The Navier-Stokes equations are the fundamental partial differential equations describing the flow of fluids with constant density for pressure changes at a constant temperature. Those fluids are called incompressible fluids.

The Navier-Stokes equations are:

$$\rho \frac{d\vec{u}}{dt} - \nabla \eta (\nabla \vec{u} + (\nabla \vec{u})^T) + \rho \vec{u} \cdot \nabla \vec{u} + \nabla p = \vec{F} \quad (2.1.1)$$

$$\nabla \vec{u} = 0 \quad (2.1.2)$$

where  $\rho$  is the fluid density,  $\vec{u}$  is the velocity vector in the x, y and z directions,  $\eta$  is the dynamic viscosity,  $p$  is pressure and  $F$  is a vector of directional forces.

This model sets changes in the particles velocity and momentum as a result of changes in pressure and dissipative viscous forces, like friction, acting inside the fluid. As we see in the equations above, all variations in velocity, and pressure set the balance of the forces acting in the fluid.

The boundary conditions of the velocity and pressure are the following:

$$\vec{u}\vec{n} = u_0 \quad (2.1.3)$$

$$p = p_0 \quad (2.1.4)$$

If we have a *no-slip* condition on a surface then the normal components of the velocity to the surface are neglected and equation (2.1.3) becomes:

$$\vec{u}\vec{n} = 0 \quad (2.1.5)$$

However this slip or symmetry condition permits changes in pressure and velocity in the boundaries and, since we will have surface restraining the fluid, the velocity in the boundary will be zero and equation (2.1.5) can be written as [17] [18]:

$$\vec{u} = 0 \quad (2.1.6)$$

## 2.1.2 Darcy's law

Darcy's law was originally determined experimentally, but can also be derived from Navier-Stokes equations via homogenization. It characterizes the flow of a fluid through homogeneous porous media by describing the relation between fluid flow, viscosity of the fluid and the pressure drop over a certain distance:

$$Q = -\frac{k \cdot A \cdot (P_b - P_a)}{\mu \cdot L} \quad (2.1.7)$$

where Q is the total flow rate in  $m^3/s$ , k is the permeability of the medium, A the cross-section area,  $\mu$  is viscosity, L length and  $(P_b - P_a)$  is the pressure drop, as shown in Figure 2.1

The permeability values depend on the material and fluid we use and it varies inversely with the fluid viscosity  $\eta$ . This leads to the coefficient  $k' = \frac{k}{\eta}$ , called intrinsic permeability, independent of the fluid used and with dimensions  $m^2$ .

If we divide equation (2.1.7) by A, and generalize the notation we end up with the following equation

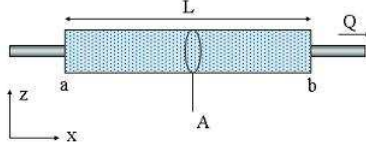


Figure 2.1: General flow diagram applied in Darcy's law.

$$q = -\frac{k}{\mu} \nabla P \quad (2.1.8)$$

where  $q$  is the flux in  $m/s$  and  $P$  is the pressure gradient vector.

To get the fluid speed in the pores, we need to relate the flux on the porosity of the medium as follows [21, 22]:

$$v = \frac{q}{n} \quad (2.1.9)$$

### 2.1.3 Brinkman equations

Brinkman equations will be used to describe the movement of fast fluids in porous media within the model. For modeling fluid flow, it is very difficult to do that in a microscopic way, because all the pores in the material are not of the same size. The behavior of the flow can be divided in two types depending on the region of the bolus we are modeling: situation with big pores and with small ones.

When the water is flowing through big holes the velocity is larger and Navier-Stokes equations for incompressible fluids may be applied. Homogeneous regions with smaller pores are considered as a permeable medium where Darcy's law is applied.

For this problem there are two conditions that must be satisfied including the continuity of the velocity and the shear stress. Since Darcy's law is not sufficient to fulfill this requirement, a generalization of it is needed and Brinkman equations make possible these boundary conditions at an interface with larger and smaller pores.

Brinkman equations are as follows:

$$\rho \frac{d\vec{u}}{dt} - \nabla \cdot \eta(\nabla \vec{u} + (\nabla \vec{u})^T) - \left(\frac{\eta}{k} \vec{u} + \nabla p - \vec{F}\right) = 0 \quad (2.1.10)$$

$$\nabla \vec{u} = 0 \quad (2.1.11)$$

where  $\rho$  is density,  $\eta$  viscosity,  $k$  permeability,  $\vec{u}$  is the velocity vector,  $p$  is pressure and  $\vec{F}$  is force.

The boundary conditions (equation (2.1.11)) are identical to the ones described for the Navier-Stokes (equation (2.1.2)) [15].

## 2.1.4 Turbulence in the flow

### Raynold's number

It has been observed experimentally that the flow in a tube can behave in two different ways: laminar or turbulent.

For a laminar flow the particles are highly ordered and the shape of the flow rate is maintained for different cross-sections along the tube. Therefore, a description of this behavior can be regarded as different concentric rings, each one with a different velocity, but increasing from zero in the most external ring touching the tube wall to a maximum in the pipe center (see Figure 2.2).

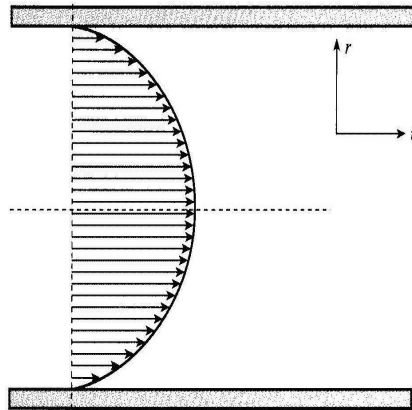


Figure 2.2: Velocity profile inside a circular pipe with laminar flow.

A turbulent flow is characterized by a high disorder, where each particle moves randomly in all directions and therefore the flow rate changes in different cross-sections along the tube, as shown in Figure 2.3.

The factor that determines which type of flow is present in the tube is expressed by the dimensionless Reynolds Number, which is given by the following equation:

$$Re = \frac{vl\rho}{\eta} \quad (2.1.12)$$

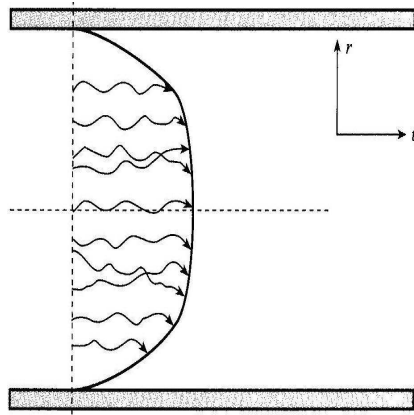


Figure 2.3: Velocity profile inside a circular pipe with turbulent flow.

where  $l$  is a characteristic length of the situation, e.g. pipe diameter,  $v$  is the velocity,  $\rho$  is the density and  $\eta$  is the dynamic viscosity.

Inside the tube there are two different forces acting on the fluid, the inertial forces, proportional to  $vl\rho$  and viscous forces, proportional to  $\eta$ . Therefore, low values of the Reynolds number characterized a laminar flow. An approximate guide to distinguish between laminar and turbulent flow would be as follows [20, 23]:

- $Re < 2 \cdot 10^3 \longrightarrow$  laminar flow
- $2 \cdot 10^3 < Re < 10^4 \longrightarrow$  transition region
- $Re > 10^4 \longrightarrow$  turbulent flow

In the next chapter this number is calculated to make a study of the flow inside the tubes.

### Flow and resistance of fluid in a tube

For the movement of the fluid in the tube, a difference in pressure between two points is needed. This pressure difference can be caused by the gravitational forces or by a water pump as the one used in this project.

For non-turbulent flow conditions ( $Re < 2000$ ) the equations describing the behavior in the tube are the so called *Poiseuille's Law* that can be described as follows:

$$Flow = \frac{Pressure}{Resistance} \quad (2.1.13)$$

$$Resistance = \frac{Viscosity \cdot Length}{Diameter^4} \quad (2.1.14)$$

$$Flow = \frac{Pressure}{\frac{Viscosity \cdot Length}{Diameter^4}} \quad (2.1.15)$$

$$Flow = \frac{Pressure \cdot Diameter^4}{Viscosity \cdot Length} \quad (2.1.16)$$

With an algebraic arrangement, equation (2.1.16) can be written as *Poiseuille's law* as follows:

$$Flow = \frac{\Delta P \cdot \pi \cdot r^4}{L \cdot V \cdot 8} \quad (2.1.17)$$

As mentioned before, over the laminar flow threshold these equations can no longer be applied [25].

When these equations are applied to the tube of our model the non-intuitive behavior of the water flowing through it can be explained. In these equations it is shown that the flow is inversely proportional to the resistance that the tube presents to the water. The larger the tube, the larger the resistance, and therefore if a hole is made in the tube most of the water flow out of this hole, since is the path with less resistance. This behavior will be shown in the next chapter.

## 2.2 Theoretical approach of the temperature distribution

To estimate the 3D temperature distribution within the system, it is necessary to calculate the heat exchange between the model and the environment. This behavior depends on the temperature difference of the two media.

The boundary temperatures are fixed for standard values, like 22°C for air. However, the temperature inside has to be determined. Since this parameter depends on the velocity of the fluid, in the case of the bolus, and on the blood perfusion in the tissue, the flow problem has to be solved prior to the thermal problem. The equations applied in the bolus are described in sections 2.1.1, 2.1.2 and 2.1.3. On the other hand, the influence of the blood flow as a heat sink is described in section 2.2.3.

The two heat flow mechanisms to be studied after having obtained the flow rate are conduction and convection. A third mechanism is radiation, but the electromagnetic power deposition is not an issue of this study and

the necessary data for this project are imported from other studies [7] and a detailed mathematical description can be found in [24].

### 2.2.1 Conduction

In the water flow to cool down, the system heat conduction takes place through oscillations of each molecule hitting the neighbors. The convection consists of the mass translation of energy through the velocity of the fluid. It is also a term used for heat dissipation from a solid into a fluid surface. This flux ( $q$ ) is characterized by a specific heat transfer coefficient ( $k_f$ ) and the temperature drop between the model ( $T$ ) and the boundaries ( $T_{ref}$ ).

$$q = k_f(T_{ref} - T) \quad (2.2.18)$$

To describe the heat transfer by conduction the *heat equation* is used.

$$\rho \cdot C \frac{dT}{dt} + \nabla \cdot (-k\nabla T) = Q \quad (2.2.19)$$

where  $T$  is temperature,  $\rho$  is density,  $C$  is the heat capacity (If it is for constant pressure  $C_p$  is used and if it is for constant volume we use  $C_V$ ),  $k$  is the thermal conductivity and  $Q$  is the heat source or heat sink [15].

If we want to calculate the final temperature distribution then there is no variation with the time and equation 2.2.19 becomes

$$\rho \cdot C \frac{dT}{dt} = 0 \quad (2.2.20)$$

### 2.2.2 Convection

If we need to include convection a term must be added in the *heat equation*

$$\rho \cdot C \frac{dT}{dt} + \nabla \cdot (-k\nabla T + \rho \cdot C_p T \cdot \vec{u}) = Q \quad (2.2.21)$$

where  $(-k\nabla T + \rho \cdot C_p T \cdot \vec{u})$  corresponds to the heat flux vector  $q$  and  $\vec{u}$  is the velocity field that can be calculated with the incompressible Navier-Stokes and Brinkman equations. If there is no convection meaning that the velocity field is zero, the heat flux vector will be as follows

$$q = -k\nabla T \quad (2.2.22)$$

The principal boundary conditions to use are the temperature ( $T_0$ ) in a boundary and the heat flux ( $q_0$ ) in it which can be set as follows

$$T = T_0 \quad (2.2.23)$$

$$-\vec{n} \cdot \vec{q} = q_0 \quad (2.2.24)$$

where  $\vec{n}$  is the normal vector to the boundary,  $\vec{q}$  is the heat flux vector and  $q_0$  is the inward heat flux normal to the boundary [15].

### 2.2.3 Penne's bioheat equation

Penne's bioheat equation is used to model the behavior in a realistic way of the tissue temperature with blood circulation of vessels diameter smaller than about 3 mm. When hyperthermia is applied, a heat sink effect is observed in tissues with high blood circulation. In this study, superficial hyperthermia is used, and since in superficial parts of the chest the vasculature is relatively small meshed, the response of the tissue to the thermal treatment is modeled with the instationary Pennes' bioheat transfer equation [7]:

$$\rho c \frac{\partial T}{\partial t} = \nabla \cdot (k \nabla T) - w_b c_b (T - T_a) + Q_S \quad (2.2.25)$$

## 2.3 Applicator model

The work conducted is basically to emulate the characteristics and conditions to make a non-invasive local hyperthermia applicator applicable. In doing this, a starting point is needed, which in this case is to determine the best conditions in which the antenna should work and to decide and appropriate model for the human body and for the system itself.

Principally, we may select between three types of models to work with as a simplification of the complicated biomass structure:

1. Planar multilayer model: human body regarded as a stratified medium composed of isotropic homogeneous lossy dielectric layers of planar geometry.
2. Spherical, cylindrical or ellipsoidal model.
3. Block model, where the biomass is considered as an assembly of a number of independent cells of lossy dielectric media.

In all calculations, the temperature of the used models will be different from the human body unless we include the flow of the blood in our calculations, because of heat dissipation in the vasculature [14]. Thus Penne's

bioheat equation has to be applied in the desired tissue as explained in subsection 2.2.3 [7].

The choice of a suitable model depends on the frequency of operation and for our frequency of operation, between 300 MHz and 3 GHz, the stratified model may be the most appropriate one. At high frequencies the depth of operation is too small, while at lower frequencies, focusing of the field is difficult. They will also produce high surface temperature because their peak temperatures are located nearer to the surface. However, this is expected since by increasing the frequency of operation, the depth of field penetration decreases the biomass. If, on the other hand, lower frequencies are used, peak temperatures will be sensed deeper in the muscle, but they will be lower, so more power will be required to achieve specified level of heating at lower frequencies [14].

The lower the operating frequency or the lower the surface temperature, the greater is the depth at which the temperature peak is located. On the other hand, the higher the surface temperature, the higher and wider is the resulting peak temperature distribution [14].

The principal frequencies used in thermal therapeutic modalities are 2450 MHz, 915 MHz and 433 MHz. Based on different results and studies, it is clear that significant advantages may be gained by choosing the 915 MHz as a compromise between the different therapeutic frequencies in use today [14]. The frequency used for the simulations of the model analyzed in this master thesis is 915 MHz [7].

Regarding the model of the instrument used for the treatment, the simplest solution we could think of would be the antenna directly attached to the skin of the patient. This solution is not acceptable because it potentially would cause undesired burns or blisters in the patient's skin [16]. Studies of electromagnetic radiated waves show that the power transfer ratio may be increased if the normally incident plane wave is made to pass through an initial layer of a low loss dielectric medium [14].

The material we use with this characteristic is denoted bolus. Besides the material properties, it is also interesting to find its appropriate thickness to obtain the best transfer ratio at the working frequency. In this study we use a 5 mm thick bolus as tested before in other studies [16], [7]. It is also very important to maintain this selected thickness throughout the volume since thinner or thicker parts could influence dramatically the overall behavior of the system [7].

Control of the surface temperature may be used to push the peak temperature deeper into the muscle, so, as mentioned in the first chapter, the use of a cooling flux through the bolus using distilled water will allow microwave hyperthermia to be produced at greater depths [16]. The temperature uni-

formity of the cooling water in the bolus is also a very relevant factor and is dependent on the shape of the applicator and the velocity of the flow. Temperature deviations in the bolus could lead to undesired heat patterns in the tissue [7].

However, a bolus with very hot water is not sufficient to produce therapeutic temperatures in the body, as will be shown in chapter 3, and therefore microwave radiators are used. As mentioned in the introduction, there are many practical advantages for using printed circuit applicators as the radiators for our model. However, we should be aware of that these applicators produce a strong electric field component perpendicular to the face of the applicator, at least in the near-field zone that includes the region likely to be used for superficial hyperthermia [14]. The microwave applicator used in this project is described in section 2.4.

So far, we have pointed out that the desired model consists of a printed antenna array radiating at a 915 MHz. The antenna produces heating to obtain a preset temperature, coupled with a low-loss dielectric material to reach an appropriate power transfer ratio, which could be a bolus, with a water flow passing through it for cooling purposes. Typically, water temperature of 42°C is used [7]. The model is shown in Figure 2.4.

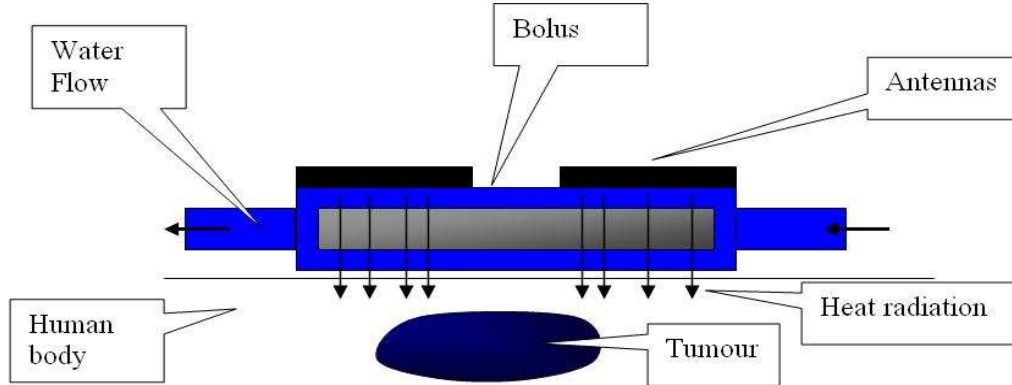


Figure 2.4: General representation of non-invasive hyperthermia model.

The part of this model I have been working on is in analyzing the water flow distribution of the bolus and the ability to maintain it at a predefined constant temperature of 42°C and observing how the flow rate influences the temperature of the tissue at a steady state. Here a prerequisite is that the temperature gradients should be minimized in the structure. To characterize the flow of freely moving fluids, Navier-Stokes equations may be used [17, 18],

which will be applied to the volumes where the water is flowing in free space. However, in these regions like in the input and output tubes, Reynold's equations should be studied to know if the behavior of the flow is turbulent or not [19, 20]. For the other parts with porous media, we could use Darcy's law [21, 22] but, since the bolus we use is not homogeneous, a more general model is needed, namely Brinkman equations [15].

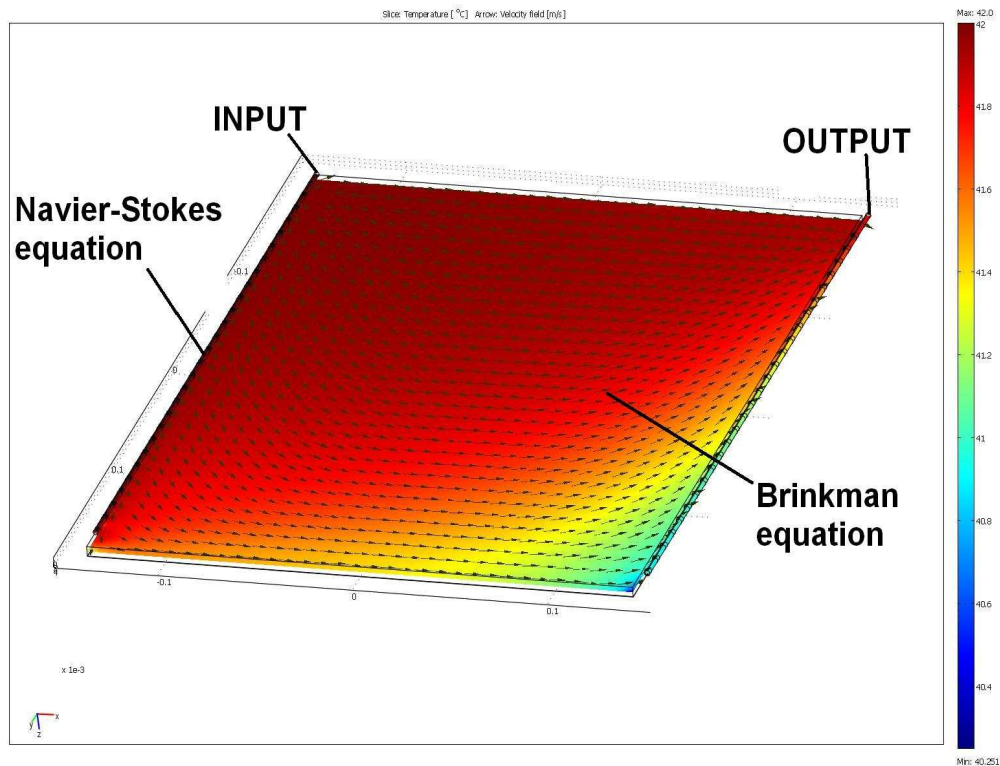


Figure 2.5: 3D model with the corresponding equations for each sub-domain.

The following sections describe the characteristics of the microwave applicators on top of the model, the theoretical laws applied in the bolus and tissue, namely the flow and temperature equations, and the computational tool used to be able to solve this model with the fluid-dynamic and thermodynamic equations.

## 2.4 Antenna applicator

This study is not focused in the electromagnetic power deposition in the tissue and therefore just relies in the data produced in other similar studies [7] and included as a heat source.

However, for a better understanding of the model it is necessary to describe which kind of applicator we are working with since, it has a very special design that makes it highly recommended for superficial hyperthermia treatments.

### 2.4.1 Antenna configuration

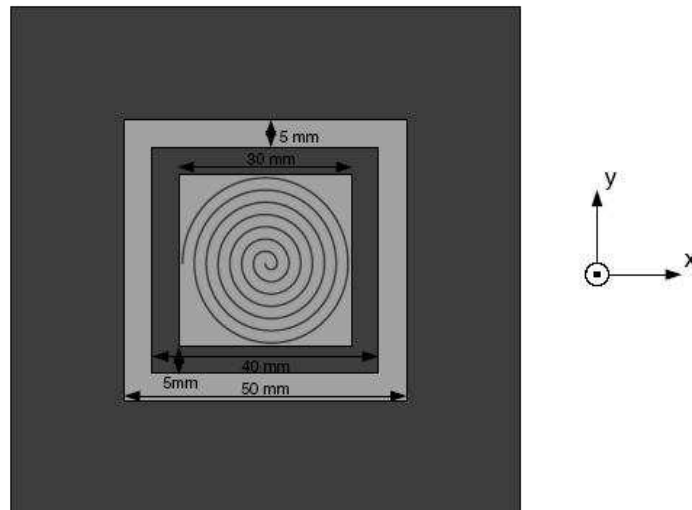


Figure 2.6: Sketch of the dual-mode transceiving antenna [7].

The antenna used is shown in Figure 2.6 and a vertical section of the whole system is depicted in Figure 2.7

It is an example of dual concentric conductor applicator (DCC) and it was introduced in the year 2001 by Rossetto and Stauffer. This specific, light, flexible, and low cost design is possible thanks to the facilities that printed circuit board (PCB) antennas give.

This antenna is designed with a double functionality of emitter and receiver and therefore can be called a transceiving antenna. The square slot DCC aperture has the functionality of heating the tissue and the central spiral

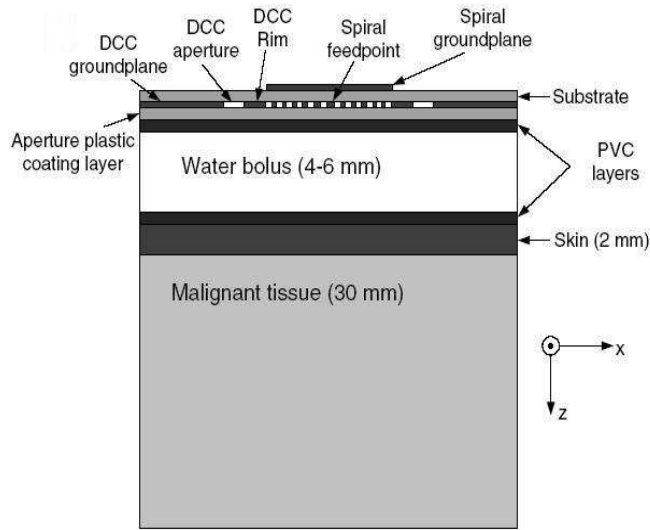


Figure 2.7: Central vertical cut of the configuration including the applicator and tissue [7].

antenna is a receiving antenna for radiometric monitoring of the temperature in the tissue under the applicator. This can make a huge improvement for hyperthermia since with radiometric thermometry, invasive temperature probes are no longer needed making the setup part of a 100% non-invasive technique [7].

## 2.5 Computational tools

To obtain an analysis of the model I have used the program package “COM-SOL Multiphysics<sup>®</sup>” [26], which is a powerful interactive environment for modeling and solving all kinds of scientific and engineering problems based on partial differential equations (PDEs). With this software, one can extend conventional models for one type of physics into multiphysics models that solve coupled physics phenomena - and do so simultaneously. That is exactly what is needed for the model mentioned above, because we face two kinds of physical problems, thermodynamics to study the temperature distribution and fluid dynamics to simulate the impact that water flow has on the temperature distribution within the volume [15].

But these are not the only tools that can be used in this program. There are many other modules that can be combined and used for basic levels of

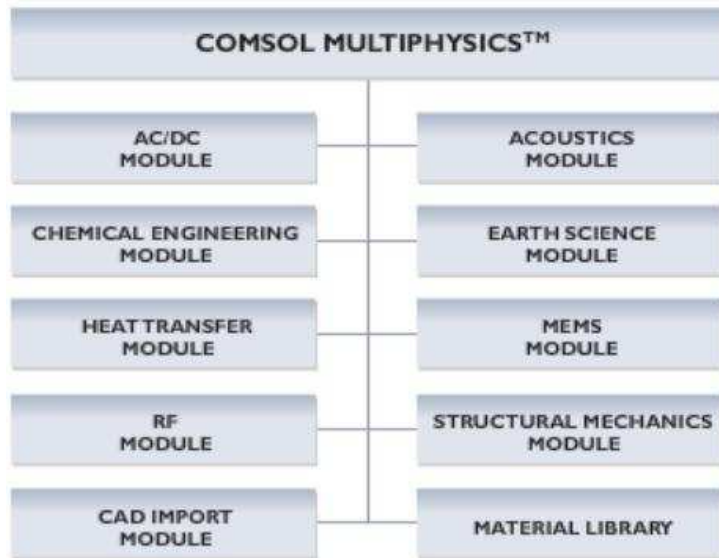


Figure 2.8: List of modules in COMSOL Multiphysics®.

education or for scientific research, as shown in Figure 2.8. From the ones shown here, the flow equations are from the Earth Science Module and the ones corresponding to thermodynamics are from the Heat Transfer Module. However, a third module has been used, which is the Cad Import Module. This module simplifies the transition from complex geometric designs created in a CAD tool to the simulation environment of COMSOL Multiphysics® [26].

The CAD tools used has been SolidWorks®. In the beginning of this project the model to be simulated was much more complicated than the one used at the end. Therefore, the drawings of a realistic model of the hyperthermia applicator had to be done in a more powerful CAD tool than the one included by COMSOL Multiphysics®. From that first model to the final one, there were 4 different attempts to draw a suitable model of the applicator, but the large amount of details and thin layers of PVC surrounding the model and keeping the water in the inside needed too many mesh elements in COMSOL Multiphysics® and the computer was running out of memory.

The biggest challenge of this project has been the meshing of the final model and the previous ones. It could be said that the 70% of the time spent to realize this master thesis has been invested in finding a proper model and its optimum meshing.

The firsts models were too complicated and close to the real applicator (Figure 2.9) but it was impossible to mesh it with less than 2 million mesh

points. With this gridding, the 16 GByte RAM computer used was insufficient and it ran out of memory.



Figure 2.9: Photo of the real model

The model was then reduced to a much simple structure made of tubes and boxes but this did not work either, since the simulations with COMSOL Multiphysics<sup>®</sup> did not show any logical results. The fluid entering to a volume from a tube stopped at the wall of the box (Figure 2.10).

The final configuration was an external tube with smaller tubes, where the hole are supposed to be, entering to the bolus. For this model a special topology and geometry had to be developed. If a normal tube is drawn in SolidWorks<sup>®</sup> with other smaller tubes coming out as shown in Figure 2.11, the amount of water entering to the volume was much larger than the one coming out.

This non-physical result was due to an inappropriate meshing of the model. The tubes had to be redesigned and built up of different small pieces drawn in SolidWorks<sup>®</sup> and imported to COMSOL Multiphysics<sup>®</sup>. The two basic parts of which the tube is made of is one simple and small tube connected together with the key part that has made possible to develop the rest of this master thesis, a “T” tube (Figure 2.12).

The final model used for the simulations consists of 27 of theses “T” tubes connected by other small tubes to build each of the lateral tubes, a central box modeling the bolus, a thin layer under the bolus modeling the plastic and a larger volume modeling the tissue under the applicator (see Figure 2.13).

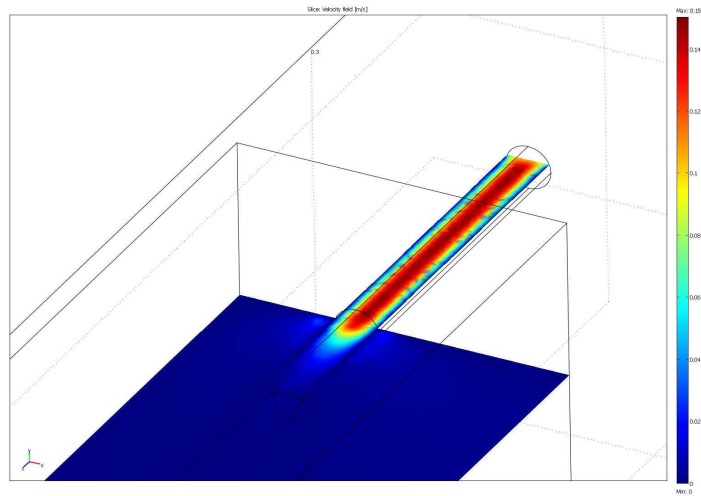


Figure 2.10: Erroneous flow simulation.

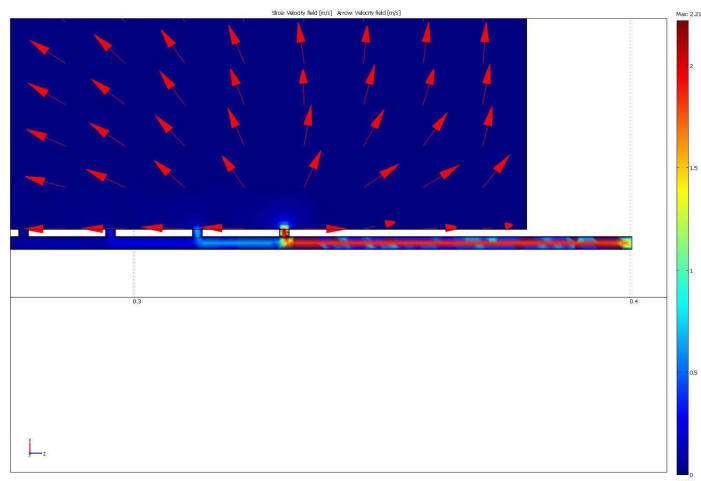


Figure 2.11: Tube architecture of previous model.

To obtain an acceptable simulation of the model with the smallest amount of mesh points possible, each volume had to be simulated individually.

First the small tubes had to be meshed by selecting one of its two faces, meshing it with the “Finer” mode and finally sweep this grid diving the volume into three parts (Figure 2.14).

Following this, the “T” tubes had to be meshed with the “*Extra – fine*”

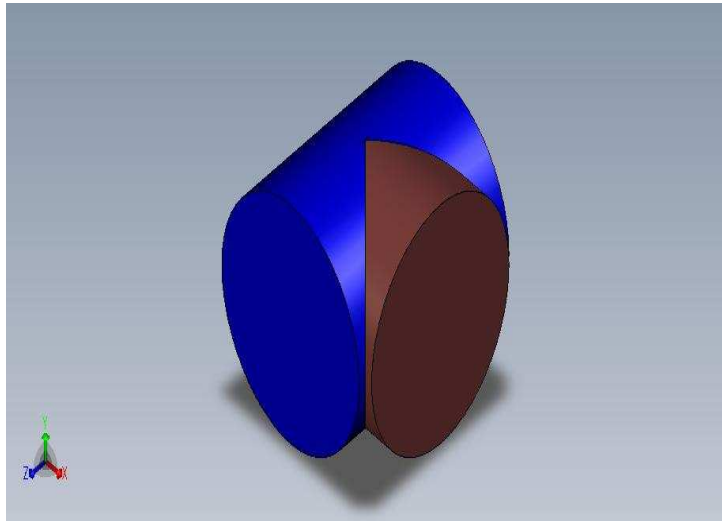


Figure 2.12: T piece of the tubes.

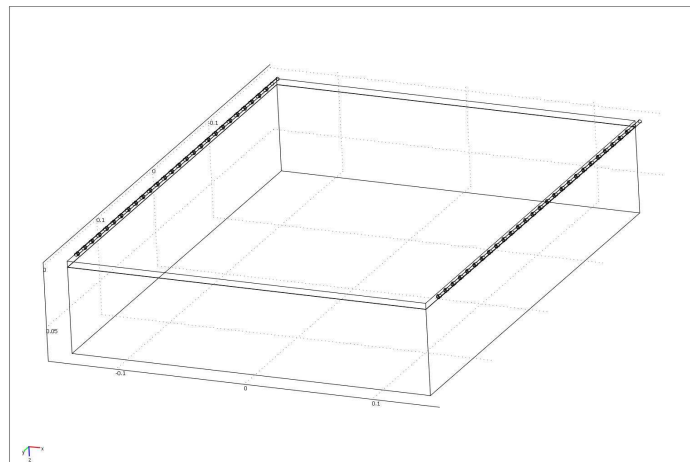


Figure 2.13: Final model.

mode (see Figure 2.15).

The central volume, the bolus, has to be meshed with the “Normal” mode and, to avoid a large increase of mesh points, the PVC layer has to be meshed swept from the bottom surface of the bolus (see Figure 2.16).

Finally the volume representing the tissue has to be meshed with the “Normal” mode. The final mesh distribution is shown in Figure 2.17. It has

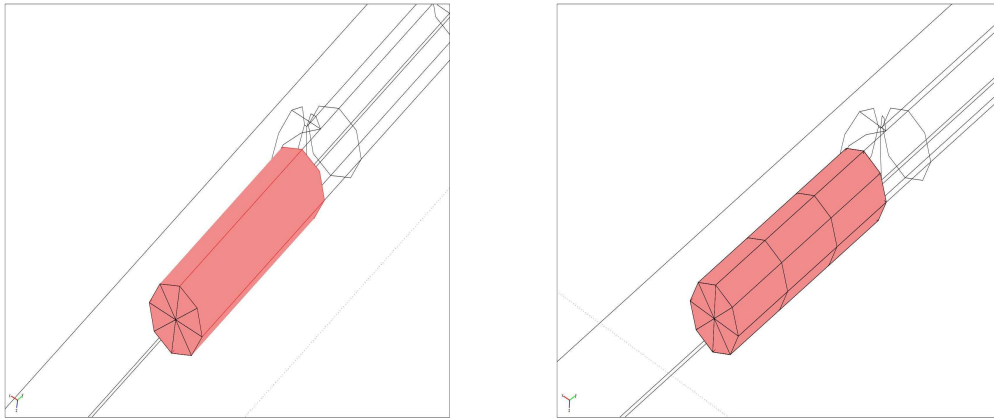


Figure 2.14: Meshing of first piece of the tube.

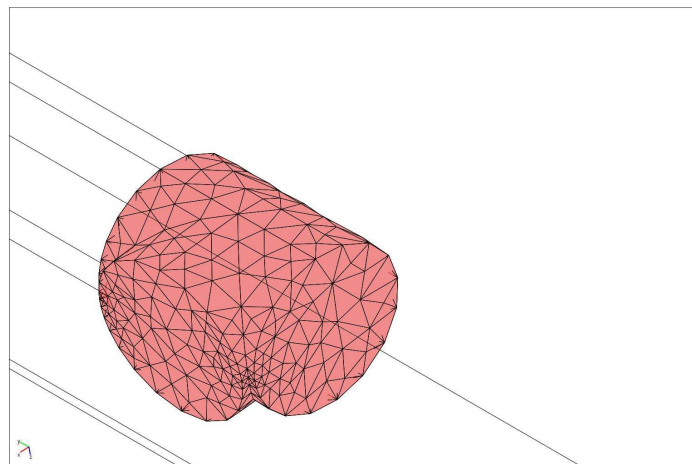


Figure 2.15: Meshing of the “T” tube.

221003 mesh elements.

To solve this model a computer with at least 6 Gigabyte of RAM memory is needed and each simulation takes about 2 hours time.

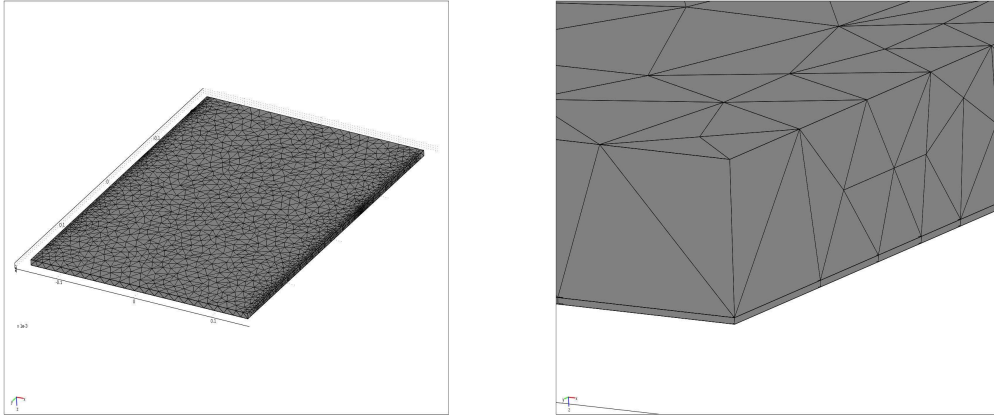


Figure 2.16: Meshing of bolus and PVC layer

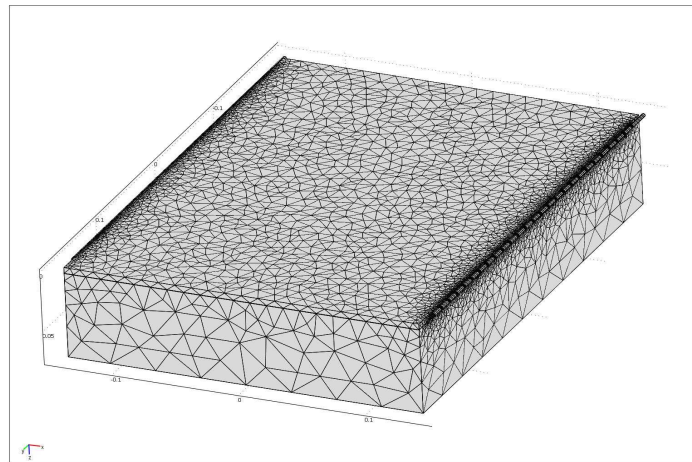


Figure 2.17: Total Meshing of the model.



# Chapter 3

## Results

In the following sections, the data taken from the simulations of the model are presented. There are several properties that should be studied and observed for a better understanding of performances of a real model. The basic sections in which this chapter is focused on are: flow in the tube, flow in the main body of the model, thermal steady state reached and influence of the microwave applicators and boundary conditions in the final temperature distribution reached in the bolus and in the tissue.

### 3.1 Tube water flow

#### 3.1.1 Raynold's number for the tube

In this project we are working with a 1.375mm radius Tygon<sup>®</sup> tube and making simulations for input velocities of 1, 5 and 10 m/s. With this characteristics, the corresponding Reynolds numbers, described in the last chapter, are:

$$Re(v_{in} = 1m/s) = \frac{vl\rho}{\eta} = \frac{1m/s \cdot 2 \cdot 1.375 \cdot 10^{-3}m \cdot 1000kg/m^3}{10^{-3} \cdot Pa \cdot s} = 2750 \quad (3.1.1)$$

$$Re(v_{in} = 5m/s) = \frac{vl\rho}{\eta} = \frac{5m/s \cdot 2 \cdot 1.375 \cdot 10^{-3}m \cdot 1000kg/m^3}{10^{-3} \cdot Pa \cdot s} = 13750 \quad (3.1.2)$$

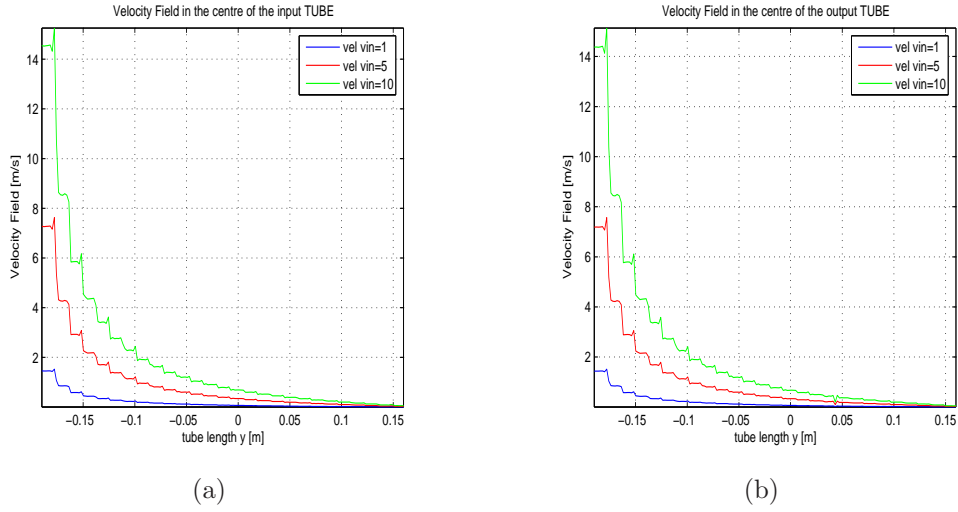


Figure 3.1: Flow rate along the input and output tubes.

$$Re(v_{in} = 10m/s) = \frac{vl\rho}{\eta} = \frac{10m/s \cdot 2 \cdot 1.375 \cdot 10^{-3}m \cdot 1000kg/m^3}{10^{-3} \cdot Pa \cdot s} = 27500 \quad (3.1.3)$$

All these values are over the laminar flow threshold, but as is shown in section 3.1.2 the simulation doesn't include the turbulence in the model.

### 3.1.2 Flow behavior in the model

In Figure 3.1 it can be seen how, both input and output tubes, experience the same water flow rate through them. Of special interest is the fact that although the construction of the tube is made with a constant hole separation there is not an homogeneous outflow of the water as explained in last chapter and as will be better analyzed in the discussion chapter.

In the previous section 3.1.1, the flow in the tube should be turbulent even for the lowest velocity. However, Figure 3.2 shows a clear laminar flow for all of them, which indicates that COMSOL Multiphysics<sup>®</sup> doesn't consider the turbulence in the flow. The question would be, how this turbulence affects to the general behavior of the model and if it is a good approximation to neglect it. For answering that, further simulations should be made. If the flow is observed once it comes out of the tube as in Figure 3.2 it can be seen how the flow decreases considerably and thus the fluid in the bolus would certainly be laminar.

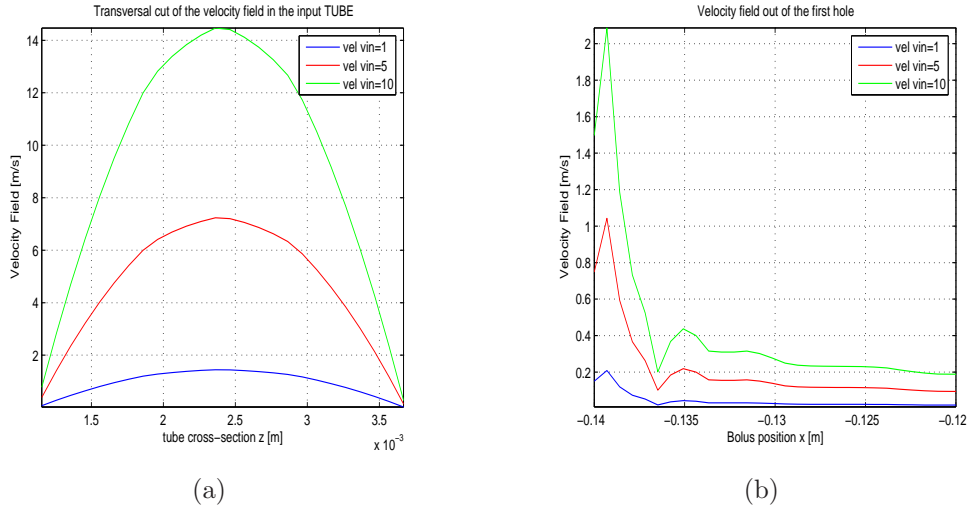


Figure 3.2: Flow cross-section and output in the first hole.

It can also be observed that the majority of the flow is pumped into the bolus through the first hole, as explained in the second chapter, and this behavior will make the flow in the bolus mainly inhomogeneous.

## 3.2 Velocity field in the bolus

The following section is one of the most important ones, since no 3D flow simulation has been reported in the literature so far for a model of such realistic shape and size. The flow will be directly responsible for the temperature distribution along the bolus and the principal tool for reaching an homogeneous temperature in it. The next simulations show the influence that the input flow rate has on the velocity field of the overall system. A further study will have to be made for choosing which one of the input velocities produce the desired performance of the model.

The model is depicted in Figure 3.3. The position of the different cross-plot sections is very important since the majority of the results taken in this project are obtained following this positioning and changing the depth at which the cuts are made.

For a better understanding of the different plots and ease the task of comparing figures, the same abscissa range is used in all of them, between  $-0.15$  and  $0.15$  m. When a plot is made along the model length (y axis) the figures are continuous but not when they are made along the model width (x axis). In this latter case, a abrupt increase in velocity is observed

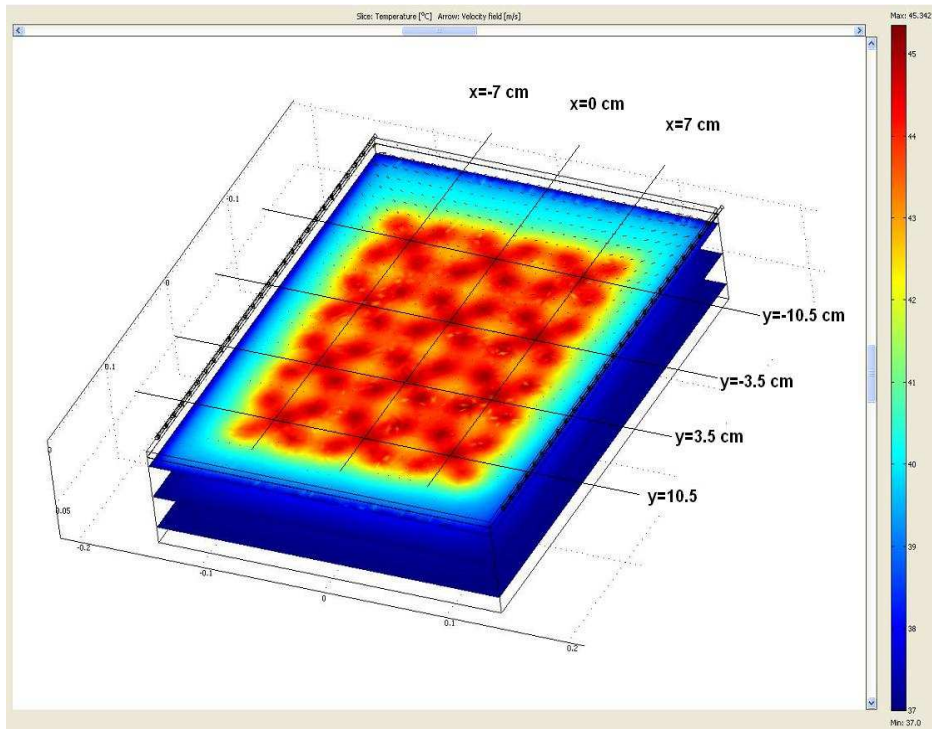


Figure 3.3: Positioning of the different lateral plot sections.

in the extremes. This increase is because the tubes are located at 0.14 m from the center of the model and the velocity is much larger there.

Figure 3.4 shows how the larger the input flow, the larger the flow in the bolus, obviously as shown in Figure 3.5. However, another important observation is that the farther from the input source, the slower the flow. Huge differences in flow can be observed and that could mean that this is not a very efficient construction, but it has to be analyzed combined with the temperature distribution before of disregarding the model.

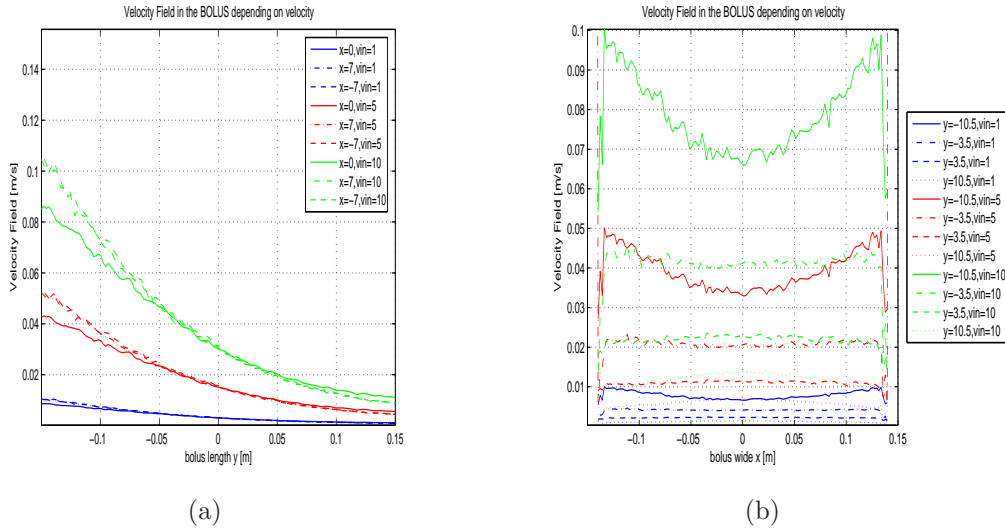


Figure 3.4: Flow rate in the y and x directions in the center of the bolus.

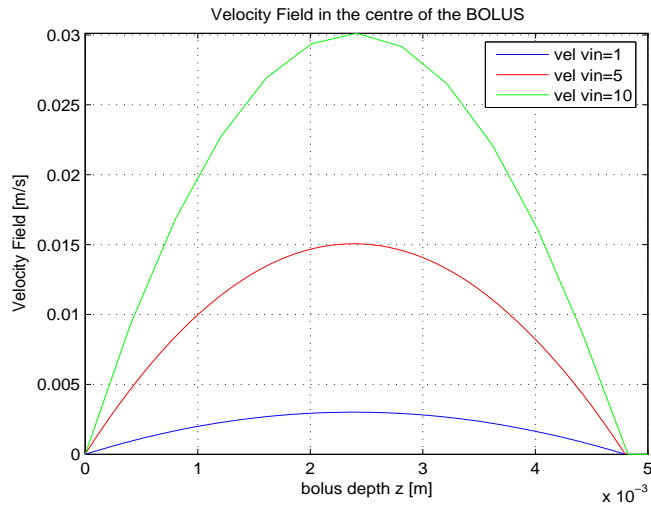


Figure 3.5: Laminar flow in the center of the bolus.

### 3.3 Temperature distribution

The goal of this project is to construct a suitable applicator for hyperthermia treatment. This goal is to be reached by heating the tumour tissue up to cytotoxic temperatures and avoid injuries to other benign tissues. Therefore a meticulous temperature analysis has to be done to control all the factor affecting the temperature distribution in the model.

For a better understanding of the different plots and ease the task of comparing figures, the same abscissa range is used in all of them, between  $-0.15$  and  $0.15$  m. When a plot is made along the model length ( $y$  axis) the figures are continuous but not when they are made along the model width ( $x$  axis). In this latter case, a sudden drop in temperature is observed in the extreme at  $0.14$  m because the lateral exit tube is reached, when studying the bolus, and approaching  $-0.14$  and  $0.14$  m when studying the tissue and skin, due to the imposed boundary condition of  $37^{\circ}\text{C}$ . The exit tube is colder due to a larger convection effect since the velocity inside is at least 10 times larger than in the bolus and is in the farthest position from the water input at  $42^{\circ}\text{C}$ .

The first step, as a comparison point, is to make a study of the model in a controlled environment and furthermore include other possible heating and cooling sources like the antennas and human tissue to clarify the specific effect of each one in the final temperature distribution.

#### 3.3.1 Temperature of the model in a controlled environment

##### Model loaded by air

In this subsection the model performance is studied when it is surrounded only by air with the subsequent heat exchange inside the model and through its environment. Figure 3.6, showing the temperature in the bolus, can be held as baseline runs and important characteristics can be observed. The higher the flow rate, the more homogeneous is the temperature distribution in the bolus. This behavior does not increase linearly, since the performance of the model for  $5$  m/s and for  $10$  m/s are very similar.

##### Model loaded by air and tissue

The heat transfer coefficient of the tissue is almost ten times bigger than the one of the air [7] and therefore a bigger exchange of heat is to be expected compared with the air-loaded case. Since the tissue is warmer than the air

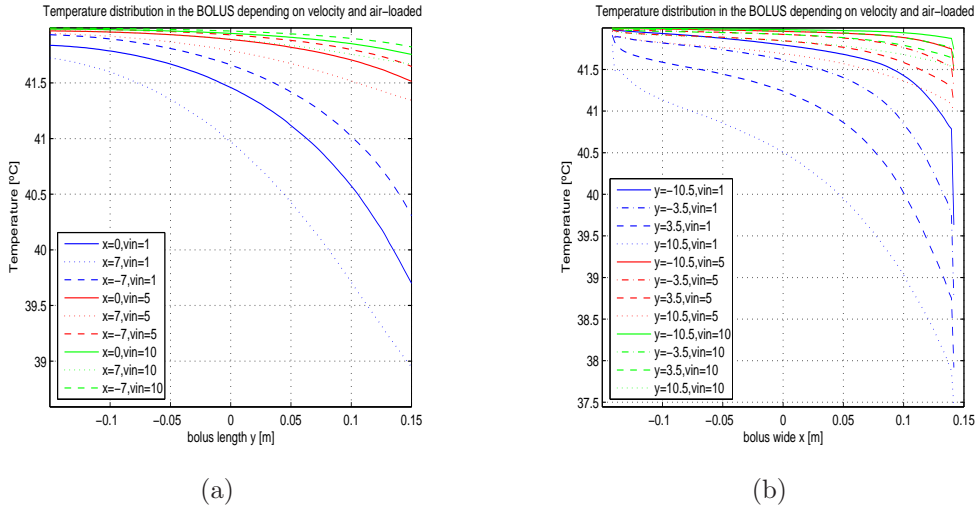


Figure 3.6: Bolus temperature distribution in the x and y direction when loaded by air.

this should lead to heating of the bolus. However this is not what is shown in Figure 3.7, because in opposition to the temperature of the tissue, the heat transfer coefficient is also ten times larger than the one of air and therefore there is a cooling effect in the bolus.

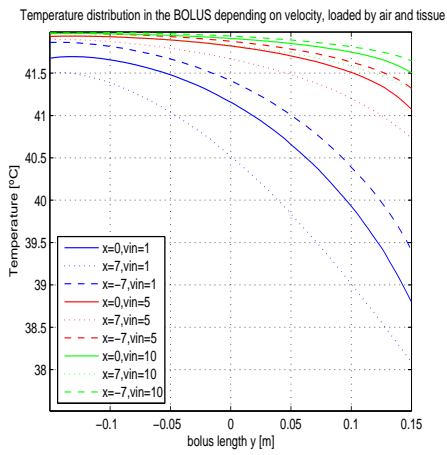
### 3.3.2 Temperature distribution of the transceiving heating antenna

The microwave applicator described in section 2.4.1 has a very characteristic heating pattern with four lobes surrounding a central maximum. This is due to the four feeding points of the antenna [7].

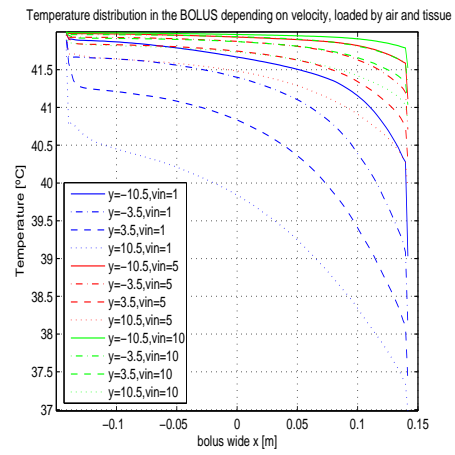
#### Heat pattern of a single antenna

A detailed study of this transceiving antenna was made by [7] and the same results are observed in this project as shown in Figure 3.8 when applied to the model. Figure 3.9 shows the temperature distribution in the bolus when a single antenna is located in the top center of the model.

In Figure 3.10 the temperature field is shown of a transversal cut in the z direction under the central antenna. There are two effects that should be pointed out. The first one is that the lowest velocity is not sufficient for maintaining the bolus at the constant desired temperature of 42°C and the second point is (as observed previously) that the performances obtained for



(a)



(b)

Figure 3.7: Bolus temperature distribution in the x and y direction when air and tissue loaded.

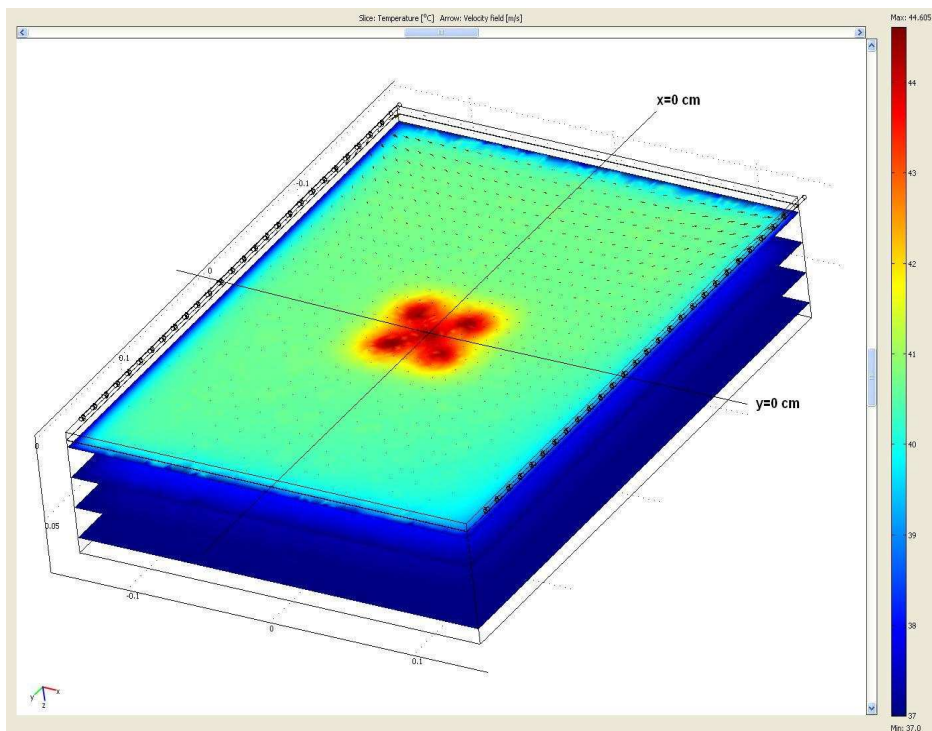


Figure 3.8: Temperature distribution for one transceiving antenna.

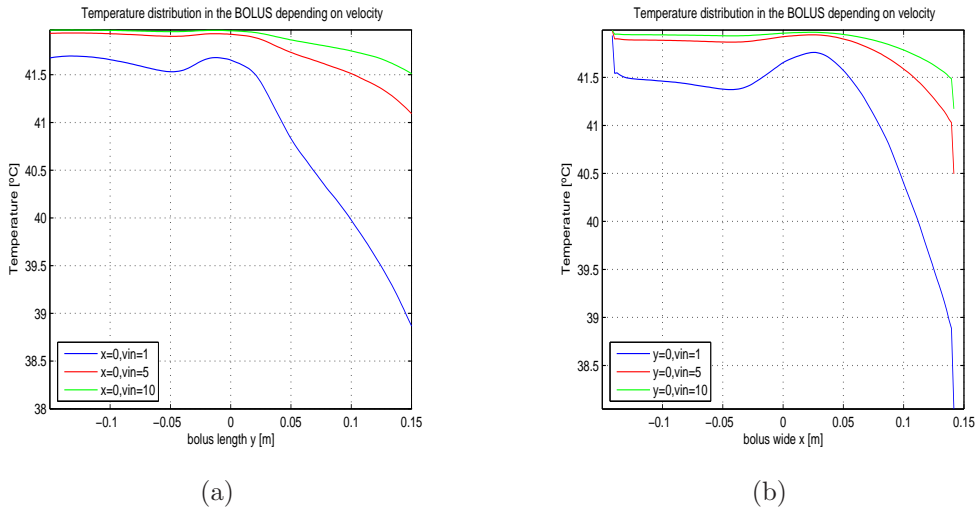


Figure 3.9: Bolus temperature distribution in the x and y direction.

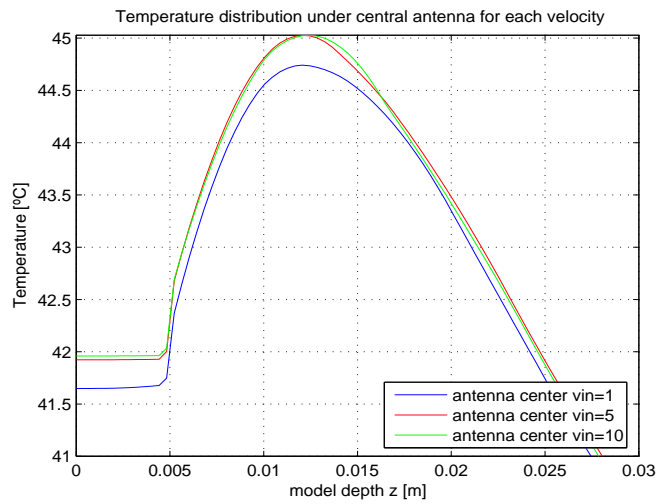


Figure 3.10: Transversal temperature section under the antenna.

5 m/s are similar to the ones of 10 m/s.

It is also important for the further composition of the antenna array to observe the temperature distribution at different depths under the lateral lobes of the antenna (Figure 3.11).

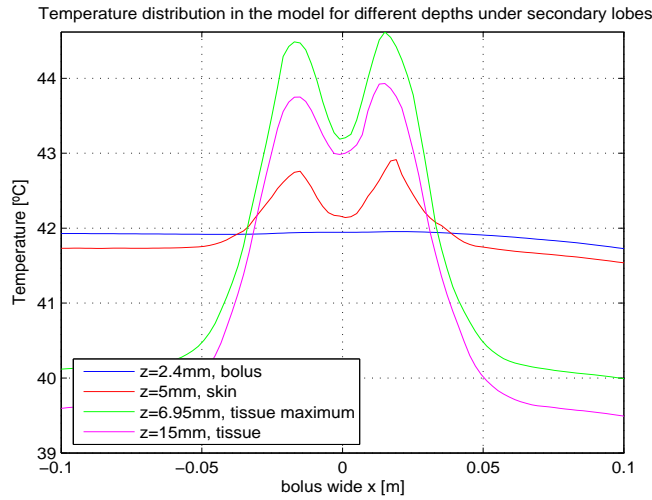


Figure 3.11: Temperature distribution at different depths under two of the lobes of the antenna.

### Skin influence on temperature distribution

As explained in subsection 3.3.1, although the tissue is warmer than the air, its larger heat transfer coefficient [7] has the effect of a heat sink in the bolus. On the other hand, since the skin acts like an isolating material between the bolus and the tissue, this latter effect is reduced and the temperature in the bolus is increased, as shown in Figure 3.12.

Once known the effect of the skin in the model, it is erased for the rest of the project, since it would only affect in the absolute values of temperature in the tissue, which are of minor importance. In this study, the most relevant issue is to study the temperature distribution in the bolus with respect to the velocity and how this velocity affects in the temperature distribution in the overall volume. Therefore the 2 mm skin is removed in order to reduce the computational load.

### Optimum antenna distribution

A clinical applicator would not consist just of a single antenna. This situation would produce a heating region in the tissue and the goal of local hyperthermia is the homogeneous heating of a transversal region and not produce located hot-spots. Therefore an array of antennas is needed.

The number of antennas is selected, due to the size of the model, 4 in the y direction and 3 in the x direction, but the optimum separation between

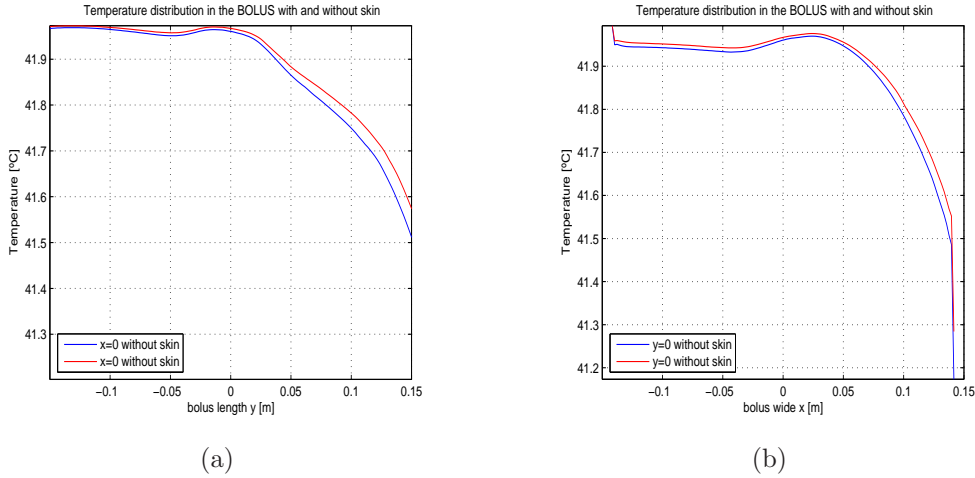


Figure 3.12: Temperature distribution for one heating antenna in the bolus with and without skin.

them has to be determined.

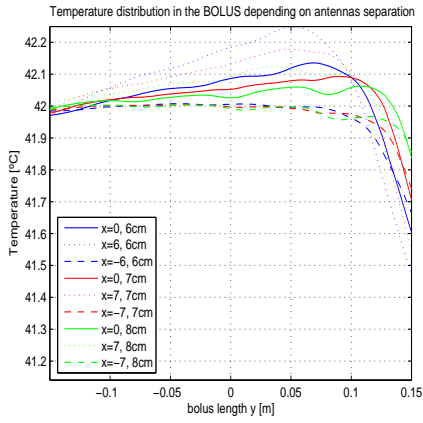
In the following figures, the temperature distribution for different depths and different antenna separations is presented. The different plots correspond to the temperature distribution under the antennas and therefore, for different antenna separation the plots are located in different positions. All of them have been made for a constant velocity.

The goal to be reached is to optimize a homogeneous temperature in each of the areas. It can be observed, comparing the figures, that the deeper we get into the tissue, the larger is the temperature differences between the peaks and the valleys.

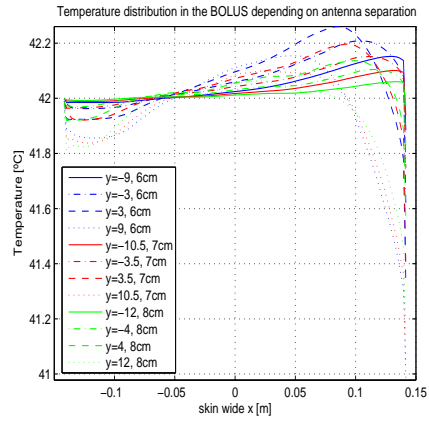
At first glance it seems that the best solution is to have the antennas as close positioned as possible. This way the difference between the peaks and the valleys is minimized and although the temperature is increased to undesired levels ( $> 45^{\circ}\text{C}$ ) this effect could be reduced by power adjustment of the antennas. However, selecting the separation of 6 cm would be a wrong choice, since it is also very important not just to observe the temperature distribution under the center of the antennas, but also under the side lobes. Figure 3.17 compares the temperature distribution at different depths for a constant velocity and different antenna separation under the secondary lobes of the transceiving antenna.

It is clear that if the antennas are distributed too close, a peak appears that can only be fixed through reduction in the power, but this would lead to undesired low temperatures in the rest of the volume.

On the other hand, when the antennas are too separated several valleys

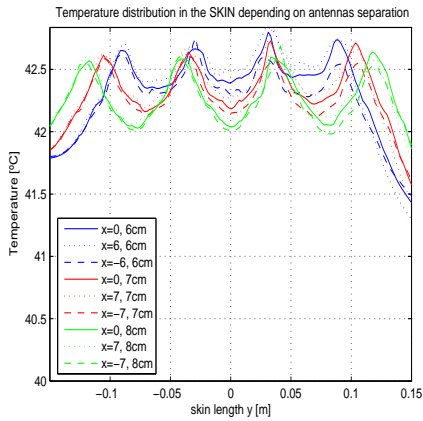


(a)

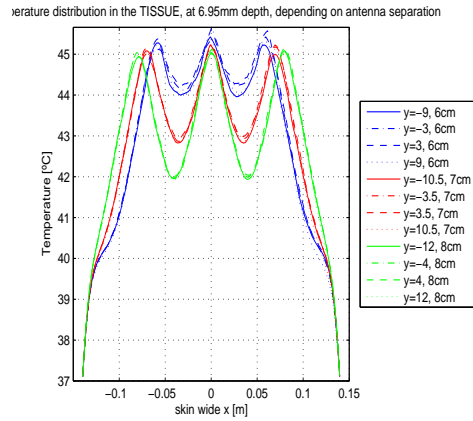


(b)

Figure 3.13: Bolus temperature distribution in the x and y direction for different antenna separation.

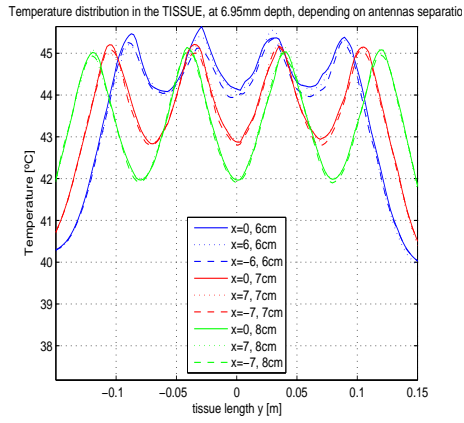


(a)

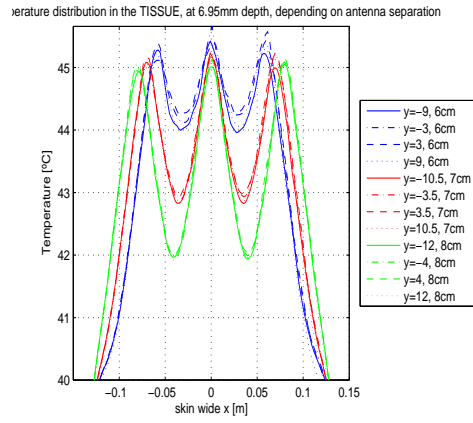


(b)

Figure 3.14: Skin temperature distribution in the x and y direction for different antenna separation.

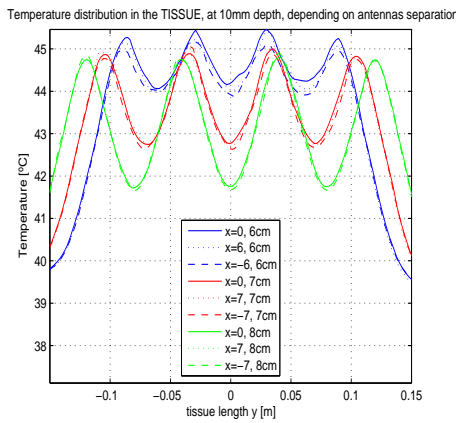


(a)

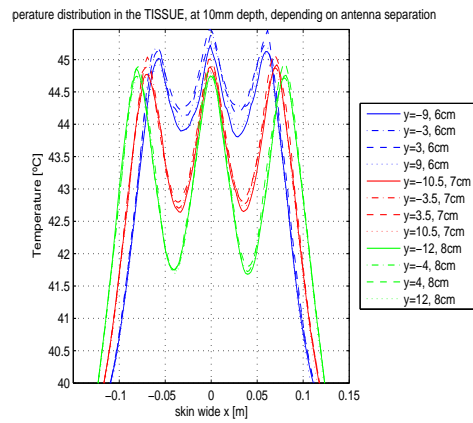


(b)

Figure 3.15: Tissue temperature distribution in the x and y direction at 6.95 mm depth for different antenna separation.



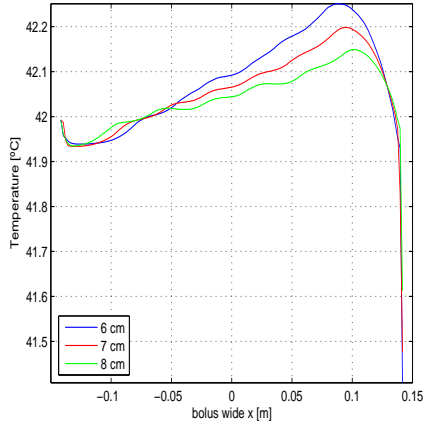
(a)



(b)

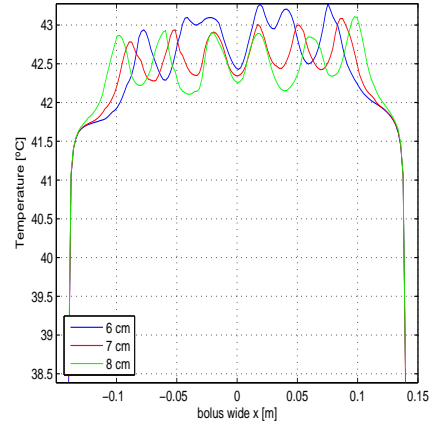
Figure 3.16: Tissue temperature distribution in the x and y direction at 10 mm depth for different antenna separation.

Temperature distribution in the BOLUS depending on antennas separation under secondary lo



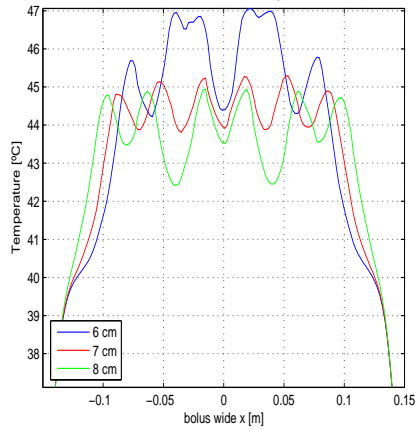
(a)

Temperature distribution in the SKIN depending on antennas separation under secondary lob



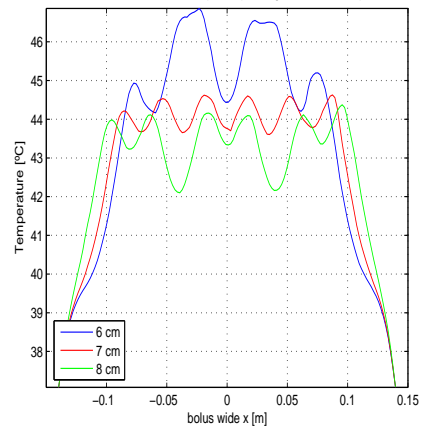
(b)

Temperature distribution in the TISSUE, at 6.95 mm depth, depending on antennas separation under sec



(c)

Temperature distribution in the TISSUE, at 10 mm depth, depending on antennas separation under sec



(d)

Figure 3.17: Temperature distribution at different depths depending on antenna separation.

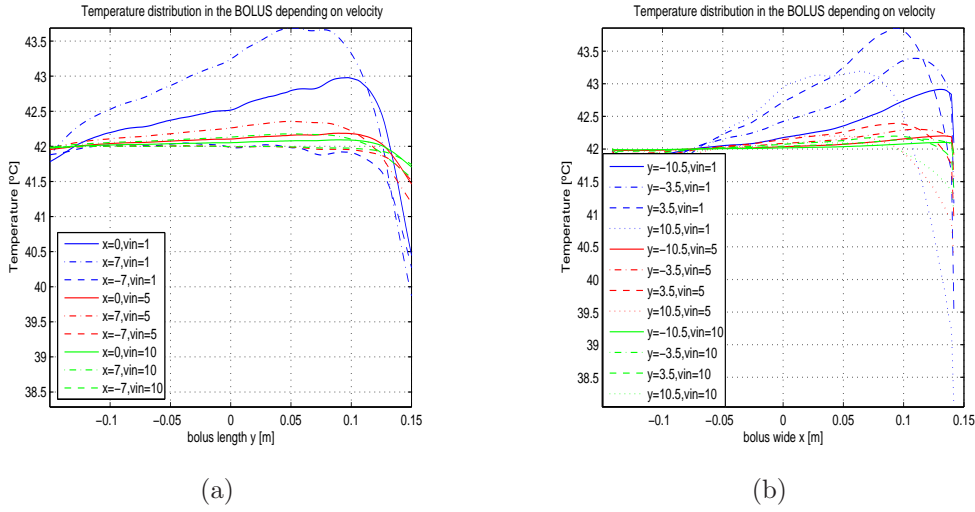


Figure 3.18: Temp in the bolus depending on the velocity.

appear that do not reached the desired temperature. This could be avoided by increasing the power, but the peaks would increase too much in temperature over the desired threshold.

Observing these results the optimum antenna separation, that is the one with the most homogeneous temperature distribution, is a separation of 7 cm.

### 3.3.3 Fluid velocity influence on temperature distribution of the final model

Once having chosen the best antenna separation for the model, it is possible to make a study of how the flow rate of the cooling water of the bolus affects the overall temperature distribution and which would be the optimum for the model. In the following figures the plots are made for the same positions as shown in Figure 3.3.

#### Lateral temperature distribution in the bolus

As shown in Figure 3.18, the higher the velocity in the bolus the more homogeneous temperature distribution in the overall volume. It is clear, that the lowest velocity of 1 m/s is not sufficient for the requirements of the hyperthermia applicator, because a too large temperature difference can be observed in the overall volume. The other two (5 m/s and 10 m/s) are very similar and the difference in temperature depending on the position is acceptable.

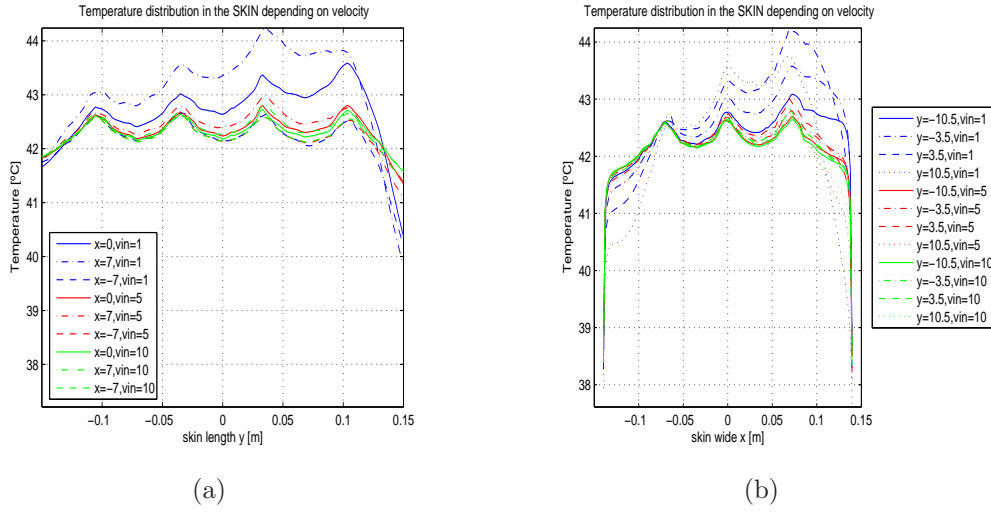


Figure 3.19: Temp in the skin depending on velocity.

### Lateral temperature distribution in the skin

In the skin it can be observed the same effects as in the bolus. Since here there is no cooling fluid (apart from the musculature), the peaks of the antennas are already visible as can be seen in Figure 3.19. At this depth, the important characteristic is not to exceed the temperature limit of  $43^{\circ}\text{C}$ , which is the pain threshold [7].

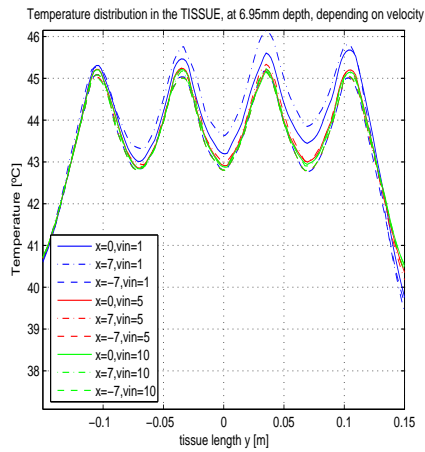
This threshold is easy to be avoided by reducing the power of the antenna, but by reducing it too much no cytotoxic temperatures are reached in the tumour.

### Lateral temperature distribution in the tissue

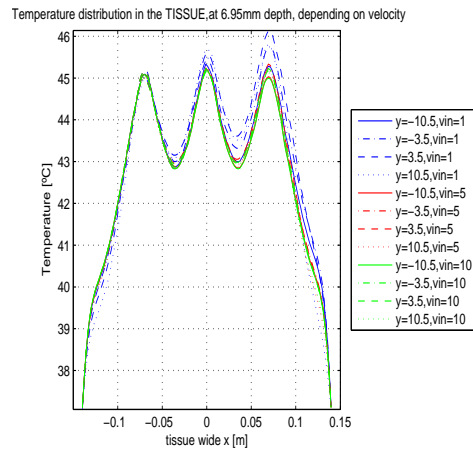
The scientific society has established the depth of 10 mm inside the tissue as a reference depth for the different hyperthermia treatments. However, in this study, data are taken from 10 mm deep and supplementary from 6.95 mm where the maximum temperature for the applied power is located.

It can be seen that the behavior of the overall system is very similar for these two depths with the only exception of a higher temperature at 6.95 mm.

Having an overall view of these figures it can be confirmed that the increase in input flow velocity from 5 m/s to 10 m/s does not substantially affect the final results.

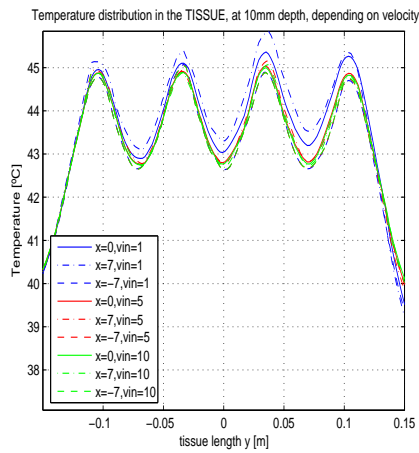


(a)

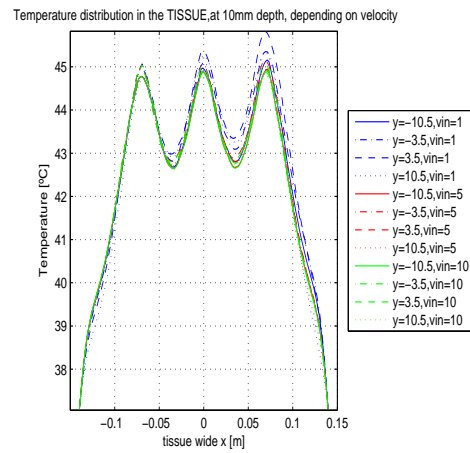


(b)

Figure 3.20: Temp in the tissue at 6.95 mm depth depending on velocity.



(a)



(b)

Figure 3.21: Temp in the tissue at 10 mm depth depending on the velocity.

## Depth temperature pattern under each antenna

The temperature distribution can be seen in Figure 3.22. The following figures are the depth profiles in the z direction, from the top of the model, where the antenna is placed and into the tissue.

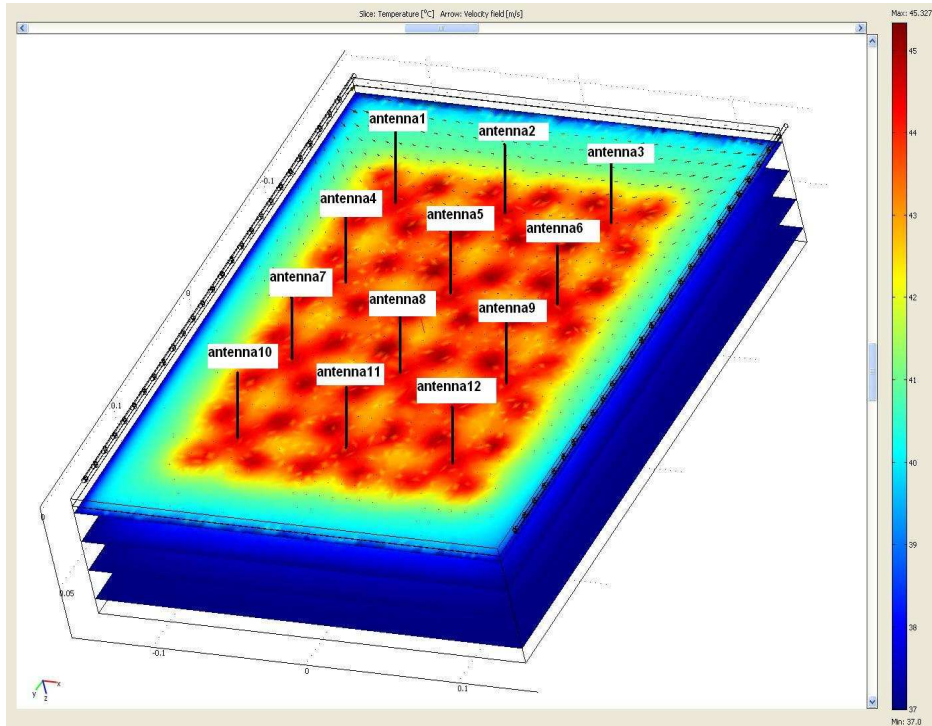


Figure 3.22: Positioning of the different transversal plot sections.

As shown in Figure 3.23 it can be seen how the velocity of the bolus affects the temperature distribution in the tissue, since the higher the flow the stronger the convection effect.

In these figures it can be observed that the higher the flow velocity the more homogeneous is the temperature in the volume, since all the lines corresponding to each antenna are closer together.

The location of the antennas and the particular transversal temperature distribution under each one is shown in Figure 3.24. This can be observed with more detail in Figure 3.25, where the plots are positioned in the same order as their respective antennas in the array.

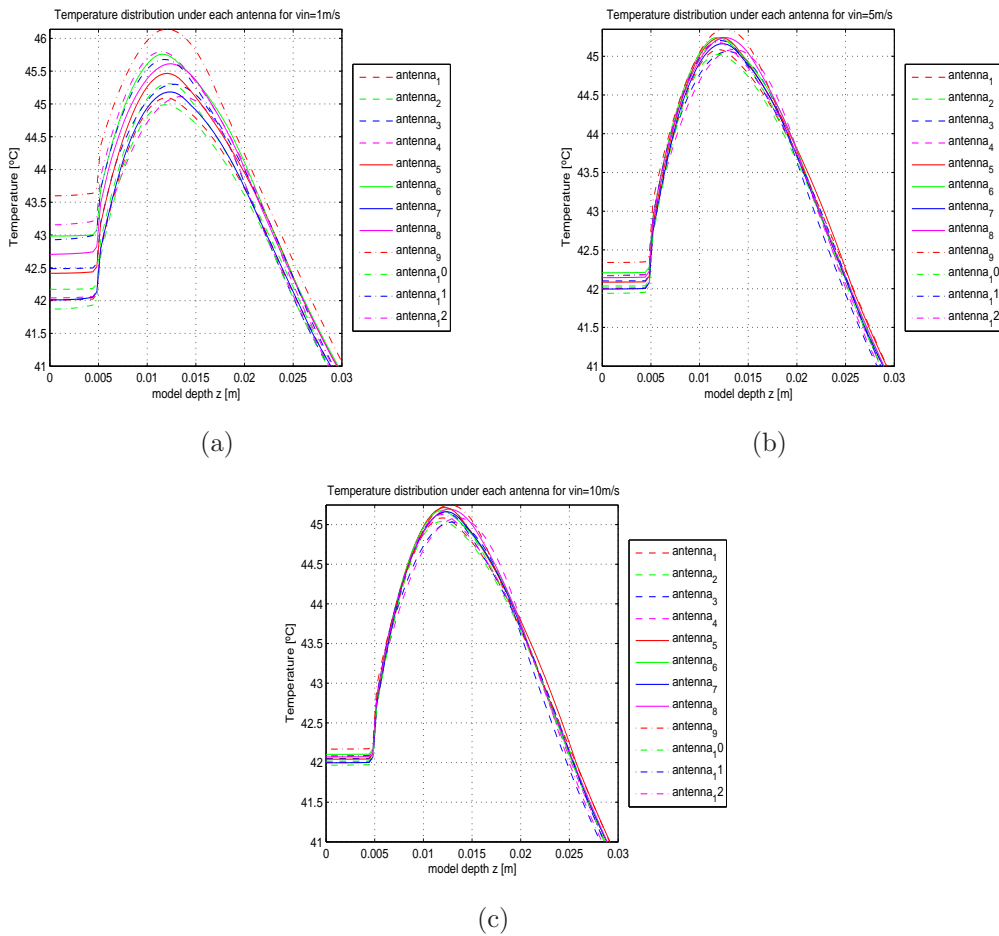


Figure 3.23: Transversal temperature distribution under each antenna depending on flow velocity.

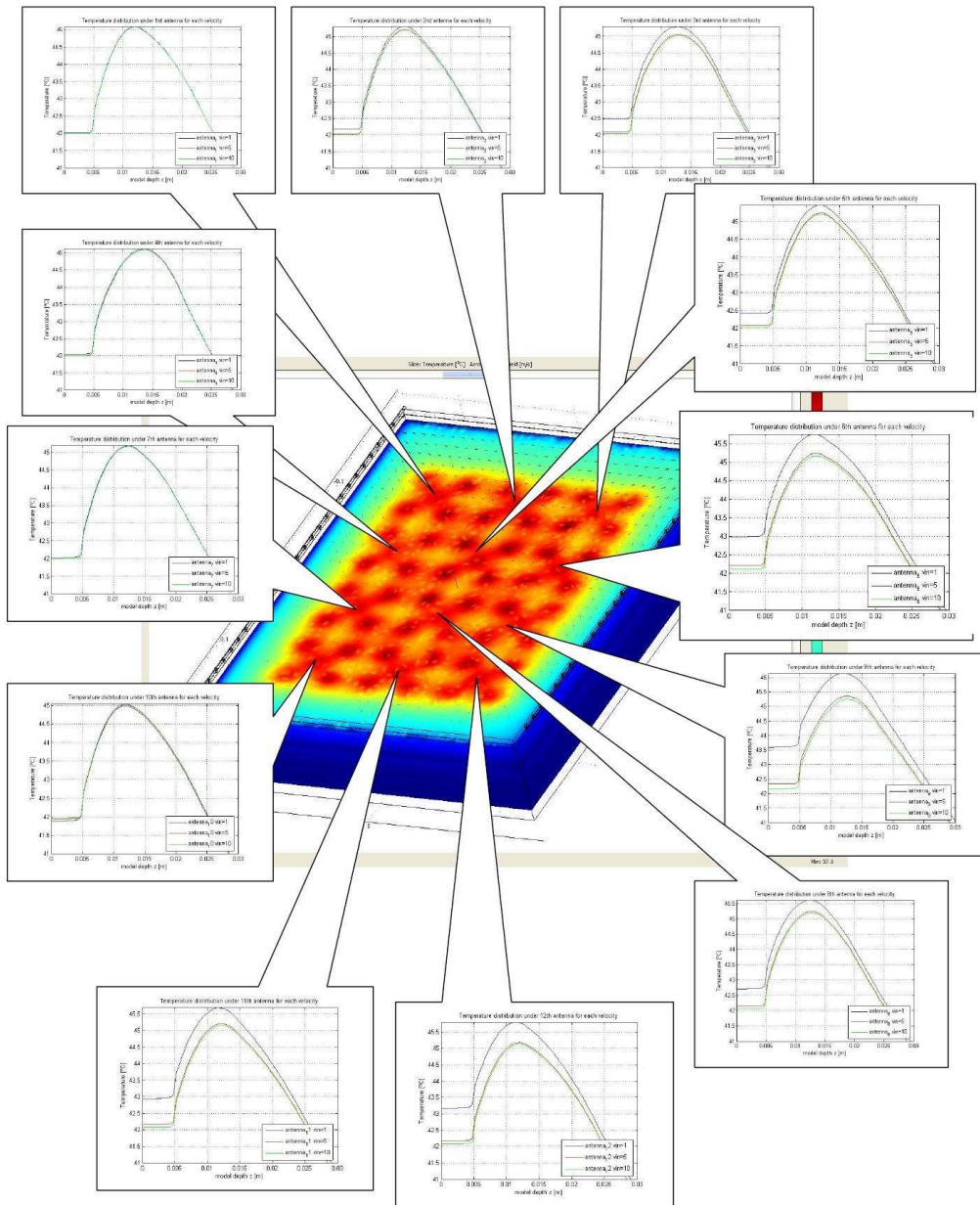
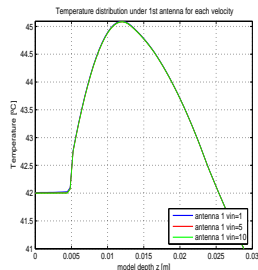
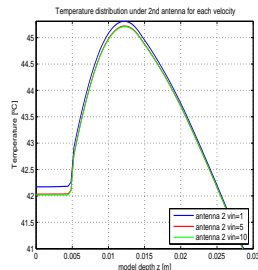


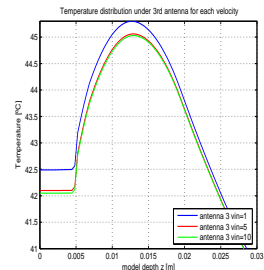
Figure 3.24: Temperature distributions in depth vs. lateral position.



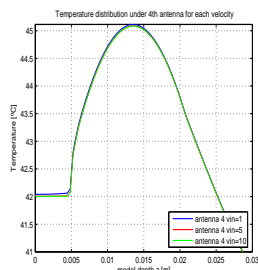
(a) antenna 1



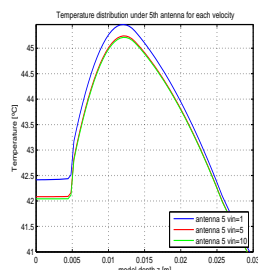
(b) antenna 2



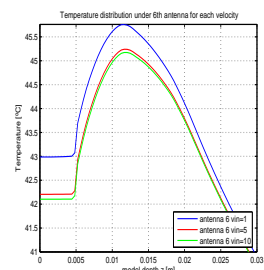
(c) antenna 3



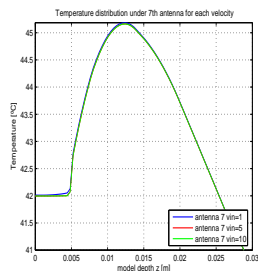
(d) antenna 4



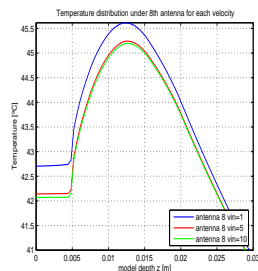
(e) antenna 5



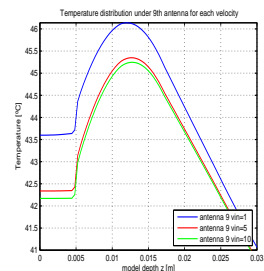
(f) antenna 6



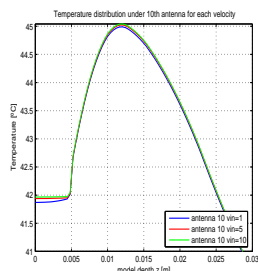
(g) antenna 7



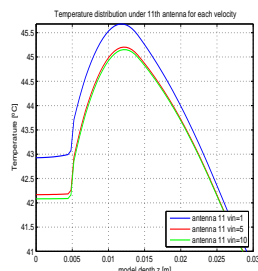
(h) antenna 8



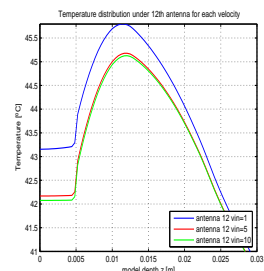
(i) antenna 9



(j) antenna 10



(k) antenna 11



(l) antenna 12

Figure 3.25: Antenna array as distributed in the model.



# Chapter 4

## Discussions

The discussion part of this master thesis follows the same structure as the results chapter. It consists of postprocessing the data obtained of the flow in the bolus and the velocity field in it, followed by a temperature analysis and description of the temperature distribution in the overall model. The final section analyzes how this latter sections can influence each other.

### 4.1 Tube water flow

In section 3.1.1 we calculate the Reynold's number for the flow in the tube, and it is observed that the flow for the different input velocities is turbulent in the entrance of the tube, since  $Re > 2000$ . However, in subsection 3.1.2 it is shown that the simulation has a laminar behavior in the entrance of the tube.

This is due to the fact that including turbulence in the flow would increase substantially the computational load of problem, since *Poiseuille's law* can no longer be applied.

The real influence of the turbulence at the entrance is not known, however as seen in figure 3.1, the fluid velocity drops very fast after each hole and also after leaving the tube and entering the bolus as shown in Figure 3.2. This means that although turbulence at the entrance, the large velocity drop sets the Reynold's under 2000 and therefore there would be laminar flow in the bolus anyway.

In Figure 3.1 it can also be seen that the flow drops to almost half its value after each hole. This is the first sign of an inhomogeneous velocity field distribution in the bolus. To avoid this, the velocity along the tube should look like a ladder, with each step equal than the one before.

## 4.2 Velocity field in the bolus

As mentioned in section 4.1, the flow along the bolus is not constant. There are two properties in the bolus flow that should be emphasized. Both are shown in Figure 3.4. Along the bolus length (Figure 3.4 a) it can be observed that the further from the source inlet, the slower is the flow. On the other hand along the bolus lateral direction (Figure 3.4 b) it can be seen, as in Figure 3.1, that the flow in the input and output tubes (extremes) are equal and it drops in the bolus center. Here, the flow is kept as laminar as seen in Figure 3.5.

The goal of this applicator is to reach an homogeneous temperature distribution in the bolus, which would be intuitively reached through a constant flow rate in the overall volume. This homogenous velocity field is not reached with this applicator design and in the next section it will be shown how this inhomogeneity influences the temperature distribution.

## 4.3 Temperature distribution

To observe how the different elements of the applicator influence the final temperature distribution an analysis part by part is made. First it is studied the boundary conditions of the bolus, and then the final model with the influence of the heat source.

### 4.3.1 Temperature of the model in a controlled environment

Intuitively, since the tissue is warmer than the air, the bolus should be warmer when loaded by air and tissue than when loaded only by air. As seen in Figure 3.6 and Figure 3.7 the effect is exactly the opposite. This is due to the conduction, as expressed in equation (2.2.18).

The temperature of the bolus (T) is around 42°C, for tissue around 37°C and of the air around 25°C. The heat transfer coefficient ( $h_f$ ) of the air is 4 and the one of the tissue is 40 [7]. This means that when COMSOL Multiphysics<sup>®</sup> makes the calculation of q (heat flux, equation (2.2.18)) in the boundary layers it would be almost 10 times larger in absolute value when loaded by tissue than when loaded by air. This results in a heat sink in the bolus due to the influence of the tissue.

## 4.3.2 Temperature distribution of the transceiving heating antenna

### Heat pattern of a single antenna

As shown in Figure 3.8 and 3.9, by placing one single antenna in the center of the bolus a central hot spot is reached in the volume surrounded by other four, where the feeding points of the antenna are located. This would be enough if the treatment studied in this project had the goal of heating only a small portion of tissue, but this is not the case. The treatment under study is local hyperthermia where the goal to be reached is to apply constant temperature in a region. Therefore an array of these antennas is needed.

From one single antenna it can be seen that a minimum velocity of 5 m/s is needed to obtain an acceptable temperature gradient along the bolus (see Figure 3.9). It is obvious that the larger the input velocity, the more homogeneous the temperature distribution in the overall volume. However, as seen in Figure 3.10 the difference between an input velocity of 5 m/s and 10 m/s is very small.

Almost all the plots of the previous chapter are made cutting under the center of the antennas. This has been chosen to make the analysis more understandable. However, for the specific task of selecting the antenna separation, a special cut under the secondary lobes of the antenna is needed.

In Figure 3.11, two of the four lobes are represented. If the goal is to obtain an homogeneous distribution, the antennas should be separated a distance so that the temperature distribution of the different antennas meet at the point where the temperature is in the middle between the peak and the region without antenna effect. A first approximation of this distance can be seen in Figure 3.11. In it, the distance between the antenna center and the middle of the temperature drop after the peak is located more or less at 3,5 cm. This means that the theoretical distance between antenna centers should be the double, 7 cm.

### Skin influence on temperature distribution

The skin has a thermal conductivity smaller than the one of the tissue. Therefore, including a 2 mm skin layer in the model would influence as an isolating layer between the bolus and the tissue. As shown in Figure 3.12 the shape of the temperature distribution with and without loading the model with a skin layer remains almost the same. The difference is very small and it is observed how including this layer increases the temperature in the bolus.

Since the only effect of the skin is in the absolute values of the final temperature distribution, this skin layer is omitted in the rest of the simulations.

The goal of this project is to study how different parameters like flow velocity affect the temperature distribution in the bolus and tissue, and not the influence on the absolute value of the temperature, since this could be reduced or increased with the power of the antenna. Therefore, to reduce the computational load of the simulation, the skin layer is omitted and many mesh elements with it.

### **Optimum antenna distribution**

Previously, a theoretical approach of the optimum antenna separation was made. In this section it is shown that if the heating pattern of the antenna was only one central lobe, then the closer the antennas, the more homogeneous would be the temperature distribution. This can be seen in Figures 3.14, 3.15 and 3.16.

The negative effect observed by placing them too close together is an increase in temperature, but this could be controlled by reducing the power of the antennas.

However, the heat power deposition pattern of the transceiving antenna used is not a single central lobe, but has other 4 secondary lobes. When temperature distribution is observed under these lobes, the temperature distributions shown in Figure 3.17 are obtained. Here, it is shown, that when the antennas are placed too close together (6 cm separation) two peaks appear in the temperature distribution. This could be solved by decreasing the power of the antennas, but this way desired therapeutic temperatures would only be reached in those two peaks.

On the other hand, when the antennas are separated too much, two large temperature drops are observed in the temperature distribution. This way is as if the antennas were working separately, and not as an array as they are supposed to, to reach a uniform temperature in the volume.

Therefore the optimum antenna separation is 7 cm. With this separation, a maximum temperature difference of 0,3°C can be observed in the bolus and about 1°C in the rest of the tissue for an input velocity of 10 m/s.

### **4.3.3 Fluid velocity influence on temperature distribution of the final model**

As it has already been mentioned, the goal is to reach a homogeneous temperature distribution in the bolus and in the tissue. There are two main tools that are the medium to reach this. One is the architecture of the model, which in this case is fixed, and the other is the input velocity. As shown in Figure 3.18, the larger the flow the more homogeneous is the temperature

pattern in the bolus. This is logical, since with a larger flow rate the renewal of the water at 42°C is faster and the heat flux through the model walls is smaller, because the temperature term “T” in equation (2.2.18) doesn’t increase.

This effect is also observed at larger depths like in the skin (Figure 3.19) and in the tissue (Figures 3.20 and 3.21). However, at these depths, the influence is not directly from the water flow, but from the heat conduction between the bolus and the tissue.

The critical point that should never be reached in the skin is the temperature of 43°C, over which the patient starts feeling pain. At the same time, a temperature of 45°C has to be reached in the malignant tissue for having a cytotoxic effect. In the results shown (Figures 3.19, 3.20 and 3.21) for the velocities of 5 m/s and 10 m/s, this goal is partially fulfilled.

In Figure 3.21 the cytotoxic temperature is reached in the peaks but not in the valleys. However, these valleys are at 43°C which could be considered also a therapeutic treatment as the one used for long term hyperthermia. These figures showing a temperature difference of 2°C are a sign showing that the square model that has been simulated should be improved to obtain also a more homogeneous temperature distribution at greater depths and not only in the bolus. However, the temperature difference is maximum here in the center of the antenna, since, when observed under the lateral lobes (see Figure 3.17), the temperature drop between peak and valley is of 1°C. In Figure 3.21 it can be appreciated again, that the results obtained by using 5 m/s and 10 m/s as input velocities are similar.

The transversal cuts presented in Figure 3.22 are made to study the penetration depth of the heat in the tissue and the temperature distribution in the bolus. In Figure 3.23 it can be observed again, that the input velocity of 1 m/s is not strong enough to reach an homogeneous temperature in the tissue, since the different plots under each antenna can be distinguished clearly from each other and some even present a temperature difference over 1°C.

On the other hand, for an input velocity of 5 m/s or 10 m/s the temperature distribution of the transversal cuts under each antenna are very similar. This points out again the observation of a similar performance in the model when using 5 m/s or 10 m/s as input velocities.

Figure 3.23 shows a desired temperature distribution, which is also the one obtained in other studies [7]. The highest temperature is located at 6,95 mm depth from the skin surface. In these simulations, it cannot be observed which are the characteristics that can influence in the depth at which the maximum is located, since for all velocities the maximum is at the same distance from the surface.

Figure 3.24 is a medium to locate the antennas in the model and therefore

understand better Figure 3.25, from which many properties of the model can be observed.

These observations are:

- The Figures show similarities and even overlapping between the temperature distributions for an input velocity of 5 m/s and of 10 m/s.
- When looking to the first 5 mm of the plots, where the bolus is located, the larger the velocity, the more homogeneous is the temperature. This is observed because for the higher velocities (5 m/s and 10 m/s) the temperature in the bolus under all the antennas is approximately 42°C.
- The farther from the input velocity source, the higher the temperature due to the heating effect of the antenna. This is logical when thinking that the farther from the input, the more time has been heated the water and therefore it is warmer.
- The velocity field drops along the bolus length (y direction), since an increase in temperature along this axis is observed. The increase in temperature is due to the fact explained in the last point (distance from the input source), but there is another effect acting here because the difference between the temperature for and input velocity of 1 m/s in the second column and the third one increases for each line. The difference between (b) and (c) is of 0,3°C, between (e) and (f) is of 0,5°C and between (h) and (i) is of 1°C. This indicates that, along the model length (y axis), the flow is less capable to release the bolus from the heat of the antennas, indicating this a decrease in velocity.

This has an exception when comparing (k) and (l) where the temperature difference is of 0,2°C. No clear explanation can be observed for this phenomenon. However a possible reason for it could be that the volume under the 12nd antenna has a lower temperature load than the rest because it is only surrounded by 3 antennas. This effect is not observed under the 10th antenna, because the water coming out of the tube is at a constant temperature of 42°C and it makes that the temperature in the bolus along the first column (Figures 3.25 (a), (d), (g) and (j)) is independent from the water velocity.

# Chapter 5

## Conclusions

### 5.1 Final conclusions about the results

The most relevant conclusion of this project would be whether the model used is a suitable model for local hyperthermia treatments or not.

The model does not fulfill all the requirements for being used as an ordinary applicator. The temperature distribution in the bolus is homogeneous although inhomogeneity in the velocity field. However, this is not applied for the tissue, where peaks and valleys have a temperature difference of up to 2°C.

This study is useful for further improvements of the model and also for correcting some non-correct suppositions that were made in previous studies [16]. In the article cited in reference 16 it is made a study of this square model and of a much ergonomic one. The only non-right supposition made is that homogeneous temperature distribution in the bolus is due to homogeneous velocity flow inside of it. In this project it has been shown that homogeneous temperature distribution is not a consequence of an homogeneous flow rate. Reference [16] follows the intuitive supposition that the flow rate coming out of the holes of the tube is equal for all of them. This has also been rejected here since the resistance and pressure inside the tube have to be taken into account (see section 2.1.4).

It is also shown that a proper velocity for the incoming water would be 5 m/s, since it offers the same performance of the model as the one of 10 m/s and it does not require all the capacity of the pumping system. This is also shared with other studies [16] where for a similar square model a flow of 4 m/s is used.

One of the challenges of this project was that it had never been done before and therefore even to find a good design to simulate was difficult. Other

negative effects were that the influence of the turbulence in the incoming tube over the volume is unknown and although Raynold's number describes the flow in the tube as turbulent (see section 2.1.4) it has been neglected in the simulation. However, after leaving the tube, the velocity decreases substantially and Raynold's number with it.

If in further simulations a significant influence of the turbulence would be proved, small changes in the model could be made to reduce these effects, like increasing the diameter of the tube.

By increasing the diameter of the tube to the double, the velocity of the input tube could be reduced 4 times maintaining the same amount of mass flowing. The relation of mass, diameter ( $d$ ) and velocity ( $v$ ) shown in Figure 5.1.1.

$$mass = constant \cdot v \cdot \rho \cdot A = constant \cdot v \cdot \rho \cdot \pi \cdot \left(\frac{d}{2}\right)^2 \quad (5.1.1)$$

where  $\rho$  is the density of the fluid. In order to maintain the mass constant, if the diameter is doubled the velocity should be 4 times smaller. By increasing the diameter to the double and reducing the velocity 4 times, Raynold's number would be reduced to half its value.

## 5.2 Further simulations and improvements in the model

Tygon tubes as the ones used in this model (see Figure 2.9) are not being used that often, specially when the shape of the bolus is different than a square, due to its restricted flexibility and because it could shift its position inside the bag affecting the flow distribution. Therefore, *heat – sealed* open water channels are used in the outer edge of the bolus with which more complicated designs can be made, as the one shown in Figure 5.1

To obtain a better performance of the square model used in this project, two things could be improved: the flow in the bolus and the antenna array distribution.

The flow could be improved, for example, by having two water inputs in the extremes of one of the tubes in order to compensate the ladder flow distribution with another ladder in the opposite direction (see Figure 3.1).

A further improvement that should be included in the simulation in the future is the influence of the gravitational force. The patient could be standing or seated and then the influence of gravity should be included. Maybe by placing the flow feeding points in the upper parts of the model (the opposite

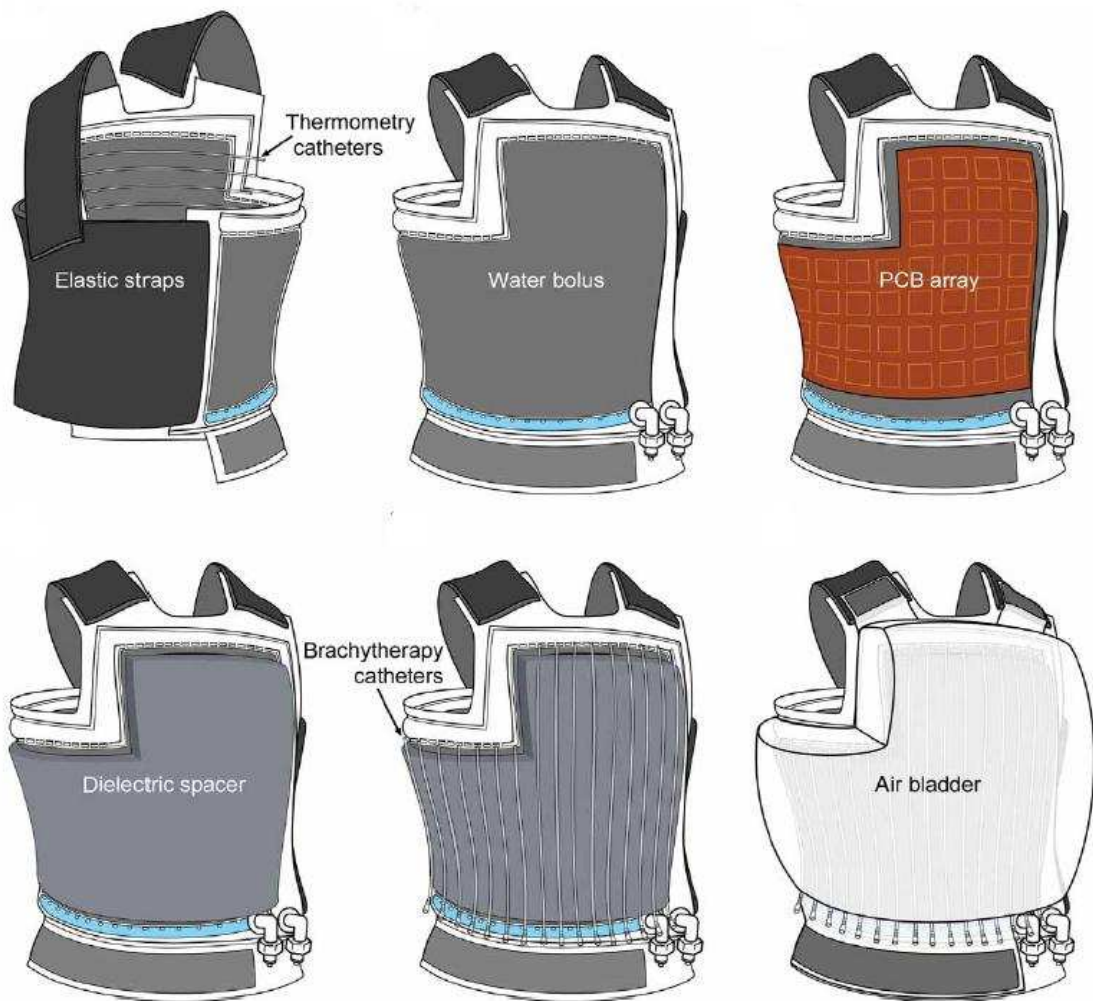


Figure 5.1: L shaped bolus with its different layers

as shown in Figure 2.9). This way the flow could be increased in the farther region from the flow input source.

It is observed in the results, that although non-homogeneous flow rate distribution, the temperature distribution is almost constant at  $42^{\circ}\text{C}$  in the bolus. The real problem lies in the tissue, where the temperature is not constant and can oscillate up to  $2^{\circ}\text{C}$ .

A possible solution for having homogeneous temperature distribution in the tissue would be to place two kinds of transceiving antennas which temperature deposition pattern would fit together as a puzzle. This might also

be done by placing some of the antennas used for the simulation turned  $90^\circ$ . The problem with it is that due to the feeding and the cables of the antennas the model would become much more complex.

One of the parameters that should be simulated in further studies is the depth of penetration and the factors affecting the position of the maximum temperature peak in the tissue. One of these factors could be the antenna power, but the most plausible ones would be the physical properties of the materials used to build the model (i.e: heat conductivity of PVC layer) or the addition of more materials coupling the PVC layer and the skin.

# Bibliography

- [1] A. Jemal, R. Siegel, E. Ward, T. Murray, J. Xu, M. j. Thun: *A cancer journal for clinicians. Cancer statistics, 2007*, American cancer society. (2007).
- [2] E. Braunwald, A. Fauci, D. Kasper, S. Hauser, D. Longo, J. J. Harrison: *Principios de Medicina Interna*, 16 ed. Madrid: Mc Graw-Hill.
- [3] S. J. Collis, S. J. Boulton: *Emerging links between the biological clock and the DNA damage response*, (2007) DOI 10.1007/s00412-007-0108-6.
- [4] E. L. Mayer, H. J. Burstein: *Chemotherapy for metastatic breast cancer*, (2007) Dana-Farber Cancer Institute, Brigham and Women's Hospital, Harvard Medical School, 44 Binney Street, Boston, MA 02115, USA.
- [5] J. J. W. Lagendijk: *Hyperthermia treatment planning*, Phys. Med. Biol. 45 (2000) R61R76.
- [6] C. J. Diederich: *Thermal ablation and high-temperature thermal therapy: overview of technology and clinical implementation*, (2007) International Journal of Hyperthermia, 21:8, 745 - 753.
- [7] S. Jacobsen, P. Stauffer: *Can we settle with single-band radiometric temperature monitoring during hyperthermia treatment of chestwall recurrence of breast cancer using a dual-mode transceiving applicator?*, Phys. Med. Biol. 52 (2007) 911-928.
- [8] M. R. Horsman, J. Overgaard: *Hyperthermia: a potent enhancer of radiotherapy*, Department of Experimental Clinical Oncology, Aarhus University Hospital, Aarhus, Denmark.
- [9] J. van der Zee: *Hyperthermia: a potent enhancer of radiotherapy*, Anals of Oncology 13: 1173-1184, 2002.

- [10] P. Wust, B. Hildebrandt, G. Sreenivasa, B. Rau, J. Gellermann, H. Riess, R. Felix, P. M. Schlag: *Hyperthermia in combined treatment of cancer*, THE LANCET Oncology Vol 3 August 2002.
- [11] A. Gevargez, D. H. W. Groenemeyer: *Image-guided radiofrequency ablation (RFA) of spinal tumors*, European Journal of Radiology (2007).
- [12] E. Chang, H. R. Alexander, S. K Libutti, R. Hurst, S. Zhai, W. D. Figg, D. L. Bartlett: *Laparoscopic Continuous Hyperthermic Peritoneal Perfusion*, (2001) American College of Surgeons.
- [13] C. Christophi, A. Winkworth, V. Muraliharan, P. Evans: *The treatment of malignancy by hyperthermia*, Surgical Oncology 7 (1999) 83-90.
- [14] R. W. Y. Habash: *Non-invasive microwave hyperthermia*, Indian institute of science, 1994.
- [15] *COMSOL Multiphysics User's guide*.
- [16] T. Juang, P. R. Stauffer, D. G. Neuman, J. L. Schlorff: *Multilayer conformal applicator for microwave heating and brachytherapy treatment of superficial tissue disease*, International Journal of Hyperthermia, November 2006, 22(7), 527 – 544.
- [17] I. L. Rhyming: *Dynamique des fluides*, 1991 PPUR.
- [18] A. D. Polyinin, A. M. Kutepov, A. V. Vyazmin, D. A. Kazenin: *Hydrodynamics, Mass and Heat Transfer in Chemical Engineering*, Taylor and Francis, London, 2002.
- [19] . Meseguer, L. N. Trefethen: *Linearized pipe flow to Reynolds number  $10^7$* , Journal of Computational Physics, 186 (2003) 187 – 197.
- [20] J. P. Bentley: *Principles of measurements systems*, Fourth Edition, Prentice Hall, 313 – 316.
- [21] H. Darcy: *Les Fontaines Publiques de la Ville de Dijon*, Dalmont, Paris (1856).
- [22] S. Stauffer, H. Philip: *Flux Flummoxed: A Proposal for Consistent Usage*, Ground Water 44 (2): 125128.
- [23] N. Rott: *Note on the history of the Reynolds number*, Annual Review of Fluid Mechanics, Vol. 22, 1990, pp. 111.

- [24] J. C. Camart, J. J. Fabre, B. Prevost, J. Pribetich, M. Chive: *Coaxial antenna array for 915 MHz interstitial hyperthermia: design and modelization-power deposition and heating pattern-phased array*, Microwave Theory and Techniques, IEEE Transactions (1992), 2243 – 2250.
- [25] S. P. Suter, R. Skalak: *The history of Poiseuille's law*, Annual Review of Fluid Mechanics, Vol. 25, 1993, pp. 1-19
- [26] [www.comsol.com](http://www.comsol.com)